2019-08-01

Pore Level Modeling of Immiscible Displacements in Heterogeneous Media

Flores de Dios Mosqueda, Tania

UNIVERSITY OF CALGARY

Pore Level Modeling of Immiscible Displacements in Heterogeneous Media

by

Tania Flores de Dios Mosqueda

A THESIS

SUBMITTED TO THE FACULTY OF GRADUATE STUDIES

IN PARTIAL FULFILMENT OF THE REQUIREMENTS FOR THE

DEGREE OF MASTER OF SCIENCE

GRADUATE PROGRAM IN CHEMICAL ENGINEERING

CALGARY, ALBERTA

AUGUST, 2019

ABSTRACT

In the petroleum industry, Reservoir Simulation plays an important role to forecast production behaviour. In this field it is essential to know the reservoir production performance under different types of exploitation. This is a key in choosing the accurate production process for a reservoir. To aim this, the main tool used for a reservoir engineer is reservoir simulation. Nowadays reservoir simulations still have some gaps such as the simulation at different scales. Commercial simulators cannot reproduce precisely the reservoir behaviour and the physics at the microscopic scale. If a reservoir simulator could be able to replicate pore scale events, they could have a more realistic representation of the reservoir physics.

This thesis tries to emulate drainage in three different 2-D heterogeneous porous media patterns with a porous plate at the production end, which restricts oil flow, but it conducts water; water being the wetting fluid and oil the non-wetting fluid.

The porous medium was inserted in an open source software for computational fluid dynamics (CFD) called OpenFOAM capable of making simulations on a micro scale and capable of reproducing pore events such as snap-off, Haines-jumps, disconnected ganglia of oil and the simultaneous filling of neighboring pores. In this thesis, graphs of the variation in fluid saturations versus time are presented in order to compare drainage process in different porous media.

ACKNOWLEDGMENT

I would like to express my sincere gratitude and admiration to my supervisor, Doctor Apostolos Kantzas who always was disposed to help me in every aspect during my residence.

I also would like to thank to my friend and colleague M. Sc. -Carla Jordana Santiago Sena for her continuous interest, support, patience and guidance during the development of the openFOAM numerical simulation code.

I appreciate the helpful support provided in the very first stage of my research to Dr. Mohammadmodari, Dr. Ghomeshi and Dr.Taheri.

NOMENCLATURE

c = scalar field

Ca = Capillary Number

$c \rightarrow f$ = linear interpolation of the volume fraction from cell centers to face centers

Cs = coefficient used on the smoothed volume fraction field

dS = surface element

e = internal energy per unit mass

E = total energy per unit mass

$f \rightarrow c$ = linear interpolation of the volume fraction from face centers to cell centers

g = body acceleration

h = enthalpy

I = identity tensor

$\bar{\bar{\mathrm{I}}}$ = the unit tensor

j = flux

K = specific kinetic energy

$\vec{\mathrm{n}}$ = normal vector

p = pressure

$\bar{\bar{\mathrm{Q}}}$s = the surface sources

q = heat flux

r = specific heat source

S = source/sink term

S_{wi} = Irreducible water saturation

u = velocity

$\vec{v}$ = the flow velocity

$\frac{|\vec{v}|^2}{2}$ = kinetic energy per unit mass

v_m = velocity field

GREEK LETTERS

$\alpha =$ volume fraction or pore radius

γ = interfacial tension (dynes/cm)

$\partial\Omega =$ closed Surface

θ = contact angle (degrees)

$\mu = viscosity\ (Pa \cdot s)$

$\rho =$ density

$\rho\vec{f}_e =$ the body force per unit volume

$\rho u\vec{v}$ = x-component of the convective flux tensor

$\rho v\vec{v}$ = y-component of the convective flux tensor

$\rho w\vec{v} =$ z-component of the convective flux tensor

σ = interfacial tensión

$\bar{\bar{\tau}} =$ viscous stress tensor

v_m = velocity field

$\emptyset$ = Porosity

$\Omega =$ control volume

ABBREVIATIONS

CCA. Conventional core analysis

CFD computational Fluid Dynamics

DNAPLs. Dense non-aqueous phase liquids

LNAPLs. Light non-aqueous phase liquids

PDEs. Partial differential equations

PIMPLE. Combined PISO-SIMPLE algorithm

PISO. Pressure-implicit split-operator

SCAL. Special core analysis

SIMPLE. Semi-implicit method for pressure-linked equations

RCA. Routine core analysis

VOF. Volume of Fluid Method

DEDICATION

WITH ALL OF ME, I DEDICATE THIS THESIS TO YOU BABY, AND FROM HERE TO THE END, IN ALL MY LIFE PROJECTS, YOU ARE GOING TO BE THE REASON OF ALL OF THEM. THANK YOU FOR BEING HERE. ELISA, THE LOVE OF MY LIFE FOR EVER.

WITH LOVE I DEDICATE THIS THESIS TO THE PERSON THAT HAS BEEN SOMETIMES SUPPORTING ME, SOME TIMES PUSHING ME, SOME TIMES BEEN PUSHED, BUT ALWAYS WITH ME, TOGETHER. THANK YOU “PITS”.

WITH ALL MY GRATITUD, MY LOVE AND ADMIRATION I DEDICATE THIS THESIS TO MY LIFE TEACHERS: MY PARENTS. YOUR TENACITY, STRENGHT, RECTITUD AND LOVE IN YOUR PROJECTS DEFINITELY MARKED MY WHOLE LIFE. I WOULD NEVER HAVE ENOUGH TIME, WORDS OR SHEETS TO EXPRESS MY INFINITE GRATITUD AND JOY FOR ALL THE GOOD MEMORIES, BOTH OF YOU WERE MY EVERYTHING.

TABLE OF CONTENTS

1 CHAPTER 1: INTRODUCTION

1.1 Fluid Accommodation in Reservoirs

The theories of the formation of oil reservoirs consider that oil traps (structural or stratigraphic) originally were filled with water. The oil and/or gas is believed to have entered the trap displacing the water to some original reservoir saturation (the irreducible water saturation). Thus, a petroleum reservoir normally contains both petroleum hydrocarbons and water occupying the same, or adjacent, pores. Quantitative evaluation of the fluids is necessary for reservoir characterization. (Tiab, D., & Donaldson 2004).

The percentage of oil and water in any given porous medium depends upon the difference in pressure between the two phases and, possibly, upon which of the two fluids was in place first. (Bruce and Welge 1947). In oil reservoirs, oil, gas and water coexist in porous media. Knowledge of the static distribution of interstitial water in oil and gas sands is of great importance in making volumetric estimates of reserves, and in the solution of dynamic-flow problems particularly (McCullough, Albaugh, and Jones 1944).

1.2 Core Analysis. Undisturbed Reservoir Information

Core is normally the only part of the undisturbed reservoir formation we can see, touch and feel at the surface. Consequently, core analysis data should be reliable and the foundation upon which integrated formation evaluation and reservoir characterization rest. Reliable and representative core analysis data are essential to calibrate and validate well logging and simulation data (McPhee, Reed, and Zubizarreta 2015).

The reliable geological interpretation of log analysis results requires a reliable definition of relationship among petrophysical and reservoir parameters of oil-gas-water-bearing rocks. Petrophysical relationships are based on the laboratory analyses of core samples saturated with formation fluids. Core analyses are conducted under surface (ambient) and subsurface (in-place or reservoir or downhole) conditions. The basic petrophysical parameters needed to evaluate a petroleum reservoir are its porosity, permeability, fluid saturation, areal extent, and formation thickness. These parameters can be estimated from three common sources: core, well logging, and pressure test analyses (Buryakovsky et al. 2012).

Core analysis involves fluid saturation measurements and petrophysical measurements on dry samples normally ambient or nominal stress and temperature conditions, whereas most measurements are made on plugs which have been conditioned and tested to reflect reservoir-appropriate saturations and often reservoir conditions.

1.3 Capillary Pressure

Capillary pressure is the differential pressure between two immiscible fluids measured in a capillary space. This concept is of several importance in petroleum reservoirs because by obtaining the capillary curves, irreducible water saturation can be obtained and the Original Oil Volume in Place can be calculated (Dullien 1992).

Capillary pressures are generated where interfaces between two immiscible fluids exist in the pores (capillaries) of the reservoir rock. It is usual to consider one phase as a wetting phase and the other as a non-wetting phase. The basic relationship between capillary pressure, interfacial tension, contact angle and pore radius is given by Laplace's Law:

$$C_p = P_n - P_w = \frac{2\gamma cos\theta}{r}$$

where;

C_p = capillary pressure (psi)

γ = interfacial tension (dynes/cm)

θ = contact angle (degrees)

r = pore radius (microns)

P_n= Pressure in the non-wetting fluid

P_w= Pressure in the wetting fluid

Conventionally, water is referred as the wetting phase since, for most reservoirs, the depositional environment is believed to have been water-filled. Thus, water-phase desaturation from 100%

saturation to S_{wir} is referred to as the primary drainage cycle, and water phase increasing from S_{wir} to S_{rnw} is referred to as the primary imbibition cycle, no matter the rock wettability. Strictly however, in an oil-wet rock, water phase decreasing is the imbibition cycle, so the definitions can be confusing.

Any element of microscopic size, cut on the interface between the two fluids occupying the pore space must be in mechanical equilibrium under the effects of the interfacial tension forces exerted on its perimeter, and of the pressure forces acting over its surface. More generally, a capillary interface is necessarily a skewed surface with a constant curvature. Concavity is always aimed toward the non-wetting fluid, otherwise the wetting angle with the solid walls cannot be respected, and the wetting fluid completely fills the pore space. As soon as the interfacial curvature is non-zero, a pressure difference reigns between the two sides of the interface. The pressure in the non-wetting fluid (*n* index) is greater than the pressure in the wetting fluid (*w* index).

Capillary pressure can be measured by several methods, though this thesis only simulates the semi-permeable membrane method which is going to be explained in detail.

1.3.1 Semi-permeable membrane method

Hydrocarbon reservoirs were initially saturated with water, which was displaced by migrating hydrocarbons and formed a trap for the oil, thus producing a petroleum reservoir. This process can be repeated in the laboratory by displacing water from a core with a gas or oil. The pressure

required for the equilibrium displacement of the wetting phase (water) with the non-wetting gas or oil is the water drainage capillary pressure, which is recorded as a function of the water saturation (Tiab, D., & Donaldson 2004).

For drainage, the model is full of water and oil gradually invades the pores according to their sizes and the availability of the nonwetting phase, until the irreducible water saturation is reached. The inlet of the system connects to the injected fluid, oil for this case. The outlet of the system connects to displaced fluid that is, the water phase.

The filling sequence depends on the pore throat size distribution of the system. It starts from the smaller capillary pressure, which is the largest throat connected to the inlet. This throat is filled with oil. Depending on the capillary pressure of the pores, the next element to be filled is either the next largest throat or the pore that connects to the throats just filled. The filling process continues until the greatest capillary pressure is achieved, the smallest throats are filled, or the irreducible water saturation is reached (Jia, Ross, and Kovscek 2007).

Difference in pressure between oil and water phases is maintained by placing one face of the core in contact with a water-wet membrane which will allow passage of water, but which will prevent escape of oil by reason of the very small diameter of its pores. The permeability of the disk should be at least 10 times lower than the permeability of the core. The pore sizes of the porous disk should be small enough to prevent penetration of the displacing fluid at a capillary pressure much higher than the one required for irreducible water saturation.

As the pressure difference between the phases is increased, a pressure is finally reached after which there is no appreciable reduction in water saturation with further increase of pressure on the oil

phase. This experiment produces a curve of capillary pressure vs. water saturation, which becomes almost vertical at some minimum water saturation. The region of this curve in which the water saturation reaches and remains substantially at a minimum has been termed “the irreducible water saturation”.

It is believed that, as oil migrates into a water-filled formation, it displaces the water from the formation, just as the water was displaced from core (Bruce and Welge 1947).

In this method care must be taken to maintain good capillary contact between the test plug and the porous plate. This is assisted by using a paste of filter-aid and brine between the plate and a filter paper. The test plug is positioned on the paper and a lead weight placed on the plug to keep it solidly in place.

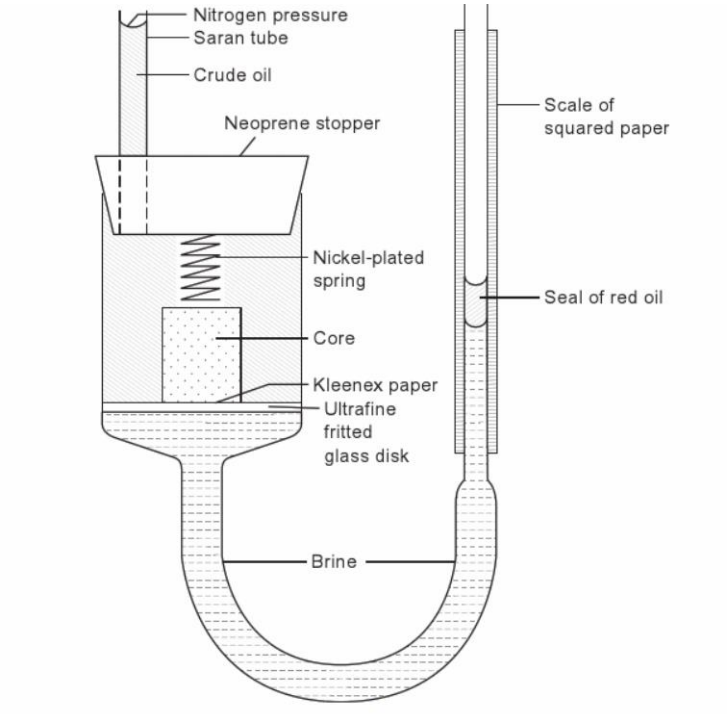

Figure 1.1 *Porous disk method for measurement of capillary pressure using a manometer* (Tiab, D., & Donaldson 2004).

Imbibition starts from the end of primary drainage. Capillary pressure decreases and water gradually invades the pores according to their sizes and the availability of the wetting phase. The element with greatest capillary pressure water connects to the porous plate, and capillary pressure is sequentially decreased. This process is more complicated and includes snap-off and piston-type displacement. Snap-off occurs when water in the pore corners swell and are no longer stable (Jia, Ross, and Kovscek 2007).

The advantages of the method are that, if the wetting characteristics are as in the reservoir, then representative data should be obtained.

Disadvantages of the porous plate method are that it is time consuming and imbibition measurements are extremely difficult (Paul Glover 2001).

1.4 Representative Elementary Volume (REV)

For the study of hydrostatics in the presence of capillary phenomena, we can define the REV (representative element of volume) as a sample of the pore space that has the minimum size required to be representative of the micromorphology of the pore space. In other words, the REV must contain a sufficient number of pores to be statistically representative of the pore size

distribution. The condition of mechanical equilibrium must be re-examined at the scale of the REV.

However, the REV will be assumed sufficiently small so that it may be possible to neglect –in its volume- the variations in hydrostatic pressure due to gravity. Taking this into account, the law of hydrostatics indicates that at the scale of the REV, the pressure in the connected phases is uniform. Capillary pressure at the interface between two connected fluids is therefore a constant. The interfacial curvature implied by Laplace's law and the wetting angle thus determines the shape of the interface that separates the two fluids, and consequently their distribution in the pore space under a given capillary pressure.

The volume of each of the two fluids is delimited inside the REV by this interface and is a function of the level of a capillary pressure. Quantitatively, this is translated by a relationship between the capillary pressure C_p and the wetting fluid volume content S_{wir}, or, more briefly, volume saturation. This is the volume of fluid contained in the REV, per unit of volume. The wetting fluid volume content is limited by the porosity. The notion of volume content of a fluid or of saturation only makes sense at the scale of the REV, contrarily to fluid pressures or capillary pressure, which can be defined in every point of a phase or of an interface. Moreover, saturation is not a state variable in the sense of thermodynamics.

In two-phase occupation, one of the two fluids is called wetting and the other is called non-wetting. The interfaces between the two fluids make a determined angle with the solids surfaces called contact angle. This angle, which is acute on the side of the wetting fluid, is the result of the affinity of each of the two fluids for the solid and is dependent on the chemical nature of each of the phases

present. In the case of prefect wetting, the wetting angle is equal to zero, and the contact of the interfaces is tangent. In this thesis all case studies are cases with perfect wetting which means that the contact angle is equal to zero.

The interface between the fluids is submitted to the phenomenon of interfacial tension. This interface behaves like a membrane under tension. Interfacial tension σ (N/m) is essentially dependent on the nature of the two fluids. The interfacial tension is constant, contrarily to the elastic tension of a membrane that depends on its own deformation. As a result, the effects of the interfacial tension only appear when the interface presents a notable curvature. In this case, interfacial tension σ=0.045 (N/m). In the pore space, strong curvatures are imposed to the interfaces as a result of the confinement of the two fluids between the solid walls, joined with the wetting angle condition.

A porous medium is composed of a solid matrix and its geometrical complement: the pore space. This pore space can be occupied by one or more fluids. The term pore space does not exempt us from discussing the definition of the word “pore” often found in the frequently used expression “at the scale of a pore” and in the common classification that distinguishes micropores, mesopores and macropores. Any criterion that defines a pore is intrinsically linked to the phenomena that are likely to occur within it. It is not hard to assign a lower limit to the size of micropores: this is the size of the smallest molecules of a fluid that can be found within in, or the typical range of van der Waals forces. Let us speak about, for example the diameter of the water molecule which is 3°A. A pore of this size is more deserving of the name absorption site used by chemists. This remains in the domain of micropores if they are cavities that can only contain a few units of small molecules of fluid, roughly up to 3nm. These are the reduced molecules of molecular dynamics. The

properties of the fluid, for example, viscosity or interfacial tension, to which these molecules normally belong, are no longer pertinent in such pores. Even the notion of pressure becomes problematic, and the intermolecular forces exerted by the solid wall play an essential role in the behavior of the populations of molecules.

We enter the domain of mesopores when the size is sufficient to contain an actual liquid phase. The liquid contained in these pores is called capillary, which means that its state (pressure) is directly linked to the interfacial tension of the liquid that exists at the interface with the surrounding atmosphere, and to the shape of the latter. The expression capillary-porous, used notably by Luikov, can be applied to porous media in which the behavior of fluids is mainly determined by the capillarity. This corresponds to macro- and mesoporous bodies, excluding microporous solids. The confinement of liquids inside the mesopores, in conjunction with the capillarity, also leads to a significant decrease in vapor pressure in comparison to the saturated vapor pressure in a free state (Daïan 2014).

1.5 Thesis Objective

The objective of this thesis is:

- To simulate reservoir charging, utilizing the porous plate as shale barrier or a cap.
- To determine trapping in primary drainage and in the presence of heterogeneities.
- To build a dynamic drainage capillary pressure curve.

1.6 Thesis Outline

In Chapter 1, Introduction, fluid accumulation in porous media and the porous plate method are briefly described.

In Chapter 2 a literature review is presented. Simulation of multiphase flow in a pore level, computational fluid dynamics and a brief description of OpenFOAM software are mentioned.

In Chapter 3, the governing equations are described.

In Chapter 4, the model setup is defined.

In Chapter 5, results and discussion can be found. They include simulation of drainage process in an immiscible displacement in eight different patterns in a water wet porous media with a porous plate at the end. Two displacements are in a homogeneous porous media, changing the displacing fluid viscosity between 1mPas and 10mPa three displacements are in a vertical heterogeneity with sensibilities to the viscosity and width heterogeneity and three displacements are in a horizontal heterogeneity with sensibilities to the viscosity and width. Graphs of pressure and fluid saturation versus time are presented and variations in pore events such as snap-off, Hanes-jumps, disconnected ganglia of oil and the simultaneous filling of neighboring pores.

In Chapter 6, conclusions and recommendations are presented.

2 CHAPTER 2: LITERATURE REVIEW

2.1 Computational porous media. A limited review

For more than six decades, multiphase flow in a pore level has been attempted to simulate using different configurations. Fatt, proposed a network of tubes as a model more closely representing real porous media. Capillary pressure curves were derived from network models and pore size distributions were calculated from those curves. In this way the difference between the true and calculated pore size distributions was shown when the capillary pressure curve was used to obtain pore size distributions for porous media (Fatt 1956). Chatzis and Dullien, (Chatzis and Dullien 1977), studied the properties of 2-D and 3-D network models of capillary tubes generalized for any pore size distribution. These properties included: (i) the breakthrough condition; (ii) the accessibility of pores; and (iii) the "pseudo" dead end pore fractions. Payatakes (DeGance and Johns 1980) developed a stochastic simulation method, which predicted the fate of solitary ganglia during immiscible displacement in water-wet unconsolidated granular porous media. This method accounted the local topology of the porous medium. These results were averaged to obtain probabilities of mobilization, breakup and stranding as functions of capillary number and ganglion size. The results from the solitary ganglion analysis were used to study the dynamics of oil bank formation. In (Mani, Mohanty, and Houston 1998), a 3-D regular cubic lattice was assumed to describe the pore space, which is formed by pore bodies (nodes) interconnected by pore throats (bonds). The bodies and throats are assumed to be spherical and cylindrical, respectively, with radii that of the largest inscribed circle in the pore. A three-dimensional (3-D) pore-level network

model was developed to calculate three-phase capillary pressure and relative permeability curves. The model combined a description of pore space morphological features and three-phase displacement physics to model capillarity-controlled gas invasion into a water-wet medium containing oil and water. Raeni (Raeini 2013), modelled multiphase flow through micro-CT images of the pore space, using OpenFOAM as a parallel open-source package for solving differential equations. He showed that the numerical model could predict various phenomena occurring in two-phase flow at the pore scale, such as snap-off in drainage and imbibition, capillary entry pressures in drainage, threshold contraction ratio for snap-off and threshold capillary number for preventing trapping in snap-off. He enabled predictions of the flow under various flow configurations at the pore scale, including co/counter-current flows and trapping/mobilization of snapped-off blobs. As a demonstration of the applicability of this concept, he applied it to successfully predict the threshold capillary number for preventing trapping of a snapped-off droplet in an imbibition simulation. He presented the relations between the forces active at the sub-pore scale to the macroscopic (Darcy-scale) pressure drops. These relations provided an unambiguous method for upscaling the numerical simulation results and calculate the relative permeability curves. He presented direct two-phase flow simulations for drainage and imbibition on sample micro-CT images of porous media at different capillary numbers and compute their relative permeability curves and their residual non-wetting phase saturations.

Carla Jordana Sena Santiago (Jordana and Santiago 2015), investigated pore-scale phenomena in two-phase flow in 2-dimensional digital porous media through direct simulations concentrated on the investigation of the ability of a Computational Fluid Dynamic (CFD) model to provide useful information regarding the physics of porous media flows. Her research demonstrated that CFD is

a powerful tool towards digital core analysis. The ability of the model to reproduce pore-scale instabilities was evaluated. Also, the model was used to investigate the balance between capillary and viscous forces at the micro-scale, providing important insights about two-phase flow in thermal recovery processes. The simulations in regular geometries (e.g., capillary tubes) were used to evaluate the optimal numerical set-up by verifying agreement with analytical solutions. In the primary drainage simulations, the main objective was to create initial water saturation in the medium, and to observe typical pore-scale events and its influence on final fluids configuration and pressure behavior. Finally, secondary imbibition simulations were used to evaluate characteristic pore-scale events and the balance between viscous and capillary forces in immiscible displacements. Sahand Etemad,(Sahand 2016) investigated phase change at the pore scale, the effect of mineral heterogeneity and surface roughness on first nucleation sites, condensation rate and film of condensation generation during steam flood at pore scale. Simulations were done with two phase flow systems both in 2-D and 3-D. Mass and heat transfer equations had to be considered simultaneously to capture complexities involved in the evaporation and condensation processes.

A numerical scheme based on the Volume-of-Fluid method was implemented using the OpenFOAM open-source CFD package along with proper phase change models. Simulations first were done in capillary tubes and a single wedge to evaluate the optimal numerical set-up by verifying with both analytical solution and experimental results. Later the third phase (oil) was introduced to the system and steam chamber growth in SAGD was modeled at the grain level. Effects of temperature on bitumen viscosity reduction during steam flooding operations as well as steam condensation at the steam-bitumen interface, trapping of the oil behind the steam front and finally countercurrent flow of steam and condensate-bitumen due to gravity were addressed.

2.2 Fluid Dynamics in a Continuous Media

Fluid dynamics is the investigation of the interactive motion of a large number of individual particles. These are in our case molecules or atoms.

Fluids that are treated as continuous media ignore the molecular structure of matter and suppose it as being without gaps or empty spaces. This hypothetical continuous material we call a continuous medium or continuum. That means, we assume the density of the fluid is high enough, so that it can be approximated as a continuum. It implies that even an infinitesimally small (in the sense of differential calculus) element of the fluid still contains a sufficient number of particles, for which we can specify mean velocity and mean kinetic energy. In this way, we are able to define velocity, pressure, temperature, density and other important quantities at each point of the fluid.

The mechanics of a continuous medium is that branch of mechanics concerned with the stressed in solids, liquids, and gases and the deformation of flow of these materials. The concept of a continuous medium permits us to define stress at a point in space conceived as occupying no volume, by a mathematical limit like the definition of the derivative in differential calculus. The theories of elasticity, plasticity and fluid mechanics based on the concept of continuous materials lead additionally to quantitative predictions which agree closely with experience over a wide range of conditions (Malvern 1969) (Tu, Yeoh, and Liu 2009).

2.3 Computational Fluid Dynamics

Most problems in fluid dynamics are too complex to be solved by direct calculation. In these cases, problems must be solved by numerical methods using computational simulations. This area of study is called numerical or computational fluid dynamics (CFD) (Jim Lucas n.d.)**.**

The history of the Computational Fluid Dynamics, started in the early 1970's. Around that time, it became an acronym for the combination of physics, numerical mathematics, and, to some extent, computer sciences all employed to simulate fluid flows. With the mid 1980's, the focus started to shift to the significantly more demanding simulations of viscous flows governed by the Navier-Stokes equations.

CFD methods are concerned with the solution of equations of fluid motion as well as with the interaction of the fluid with solid bodies. The equations governing the motion of an inviscid fluid are the Euler equations and of the viscous fluid are the Navier-Stokes equations.

Two qualitatively distinct types of viscous fluid flows are encountered in general: laminar and turbulent. The solution of the Navier-Stokes equations does not raise any fundamental difficulties in the case of laminar flows. However, the simulation of turbulent flows continues to present a significant challenge as before. A relatively simple way of modelling turbulence is offered by the so-called Reynolds-averaged Navier-Stokes equations (Blazek 2005).

2.4 OpenFOAM; a CFD Software

OpenFOAM is a C++ library, used primarily to create executables, known as applications. The applications fall into two categories: solvers, that are each designed to solve a specific problem in continuum mechanics; and utilities, that are designed to perform tasks that involve data manipulation. OpenFOAM contains numerous solvers and utilities covering a wide range of problems.

OpenFOAM is free and open source CFD software. It has a large user base across most areas of engineering and science, from both commercial and academic organizations. OpenFOAM has an extensive range of features to solve anything from complex fluid flows involving chemical reactions, turbulence and heat transfer, to acoustics, solid mechanics and electromagnetics.

OpenFOAM is free software, it means that users have the freedom to run, copy, distribute, study, change and improve the software. Being open source is a precondition for some of these freedoms, such as allowing study and change of the software and redistribution of modified software. It is this combination of code transparency and public scrutiny that makes open source software reliable, robust and effective. A good example is the Linux kernel which forms the basis for the Linux operating system used extensively in computer servers and embedded devices, and the Android operating system used for tablet computers and smartphones. OpenFOAM has an extensive range of features to simulate anything from turbulent flows in automotive aerodynamics, to fires and fire suppression in buildings, involving combustion, chemical reactions, heat transfer,

liquid sprays and films. It includes tools for meshing in and around complex geometries (e.g. a vehicle), and for data processing and visualization, and more. Almost all computations can be executed in parallel as standard to take full advantage of today's multi-core processors and multi-processor computers.

OpenFOAM is supplied with pre- and post-processing environments. The interface to the pre- and post-processing are themselves OpenFOAM utilities, thereby ensuring consistent data handling across all environments. In order to understand the way in which the OpenFOAM works, some background knowledge of C++, the base language of OpenFOAM, is required. The overall structure of OpenFOAM is shown in **Figure 2.1**

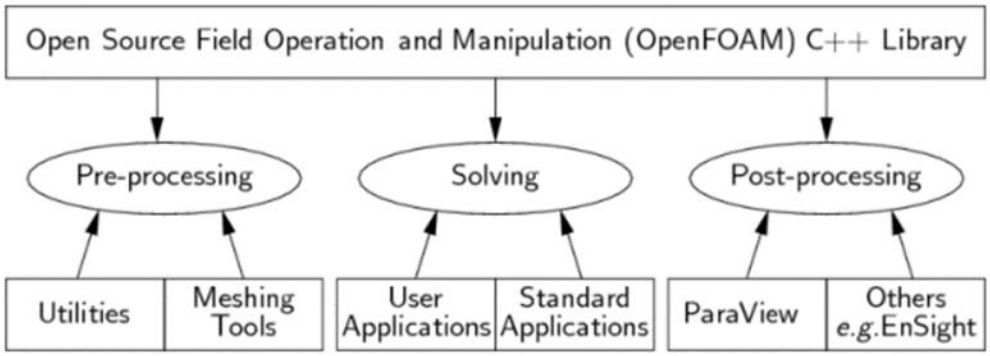

Figure 2.1 *Overview of OpenFOAM structure* (CFD DIRECT2018)

2.5 OpenFOAM Structure

The basic directory structure for an OpenFOAM case, that contains the minimum set of files required to run an application, is shown in ***Figure 2.2*** and described as follows:

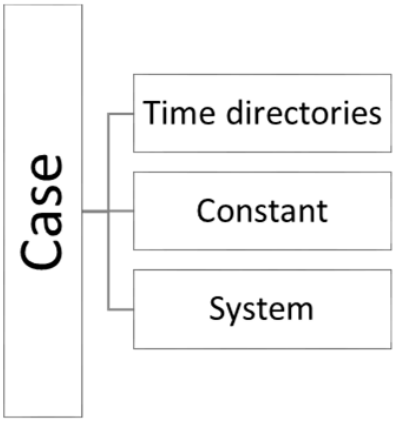

Figure 2.2 *Case directory structure*

2.5.1 The ‘time’ directories

These directories contain individual files of data for particular fields. The data can be: either, initial values and boundary conditions that the user must specify to define the problem; or, results written to file by OpenFOAM. Note that the OpenFOAM fields must always be initialized, even when the solution does not strictly require it, as in steady-state problems. The name of each time directory is based on the simulated time at which the data is written. It is sufficient to say now that since we usually start our simulations at a given time, the initial conditions are usually stored in a directory named 0 or 0.000000e+00, depending on the name format specified.

2.5.2 Constant directory

It contains a full description of the case mesh in a subdirectory polyMesh and files specifying physical properties for the application concerned.

2.5.3 System Directory

It sets the parameters associated with the solution procedure itself. It contains at least the following 3 files: controlDict where run control parameters are set including start/end time, time step and parameters for data output; fvSchemes where discretization schemes used in the solution may be selected at run-time; and, fvSolution where the equation solvers, tolerances and other algorithm controls are set for the run (CFD Direct 2018).

3 CHAPTER 3. GOVERNING EQUATIONS

The derivation of the principal equations of fluid dynamics is based on the fact that the dynamical behavior of a fluid is determined by the following conservation laws, namely:

1. the conservation of mass,
2. the conservation of momentum, and
3. the conservation of energy.

The conservation of a certain flow quantity means that its total variation inside an arbitrary volume can be expressed as the net effect of the amount of the quantity being transported across the boundary, of any internal forces and sources, and of external forces acting on the volume. The amount of the quantity crossing the boundary is called flux. The flux can be in general decomposed into two different parts: one due to the convective transport and the other due to the molecular motion present in the fluid at rest. This second contribution is of a diffusive nature it is proportional to the gradient of the quantity considered, and hence it will vanish for a homogeneous distribution. As we do not have heat transfer, nor heat sources, the conservation of energy is not going to be mentioned below.

The discussion of the conservation laws leads us quite naturally to the idea of dividing the flow field into a number of volumes and to concentrate on the modelling of the behavior of the fluid in one such finite region. For this purpose, we define the so-called finite control volume and try to develop a mathematical description of its physical properties.

3.1 Finite Control Volume

Consider a general flow field as represented by streamlines in ***Figure 3.1*** An arbitrary finite region of the flow, bounded by the closed surface $\partial\Omega$ and fixed in space, defines the control volume Ω. We also introduce a surface element dS and its associated, outward pointing unit normal vector $\vec{n}$.

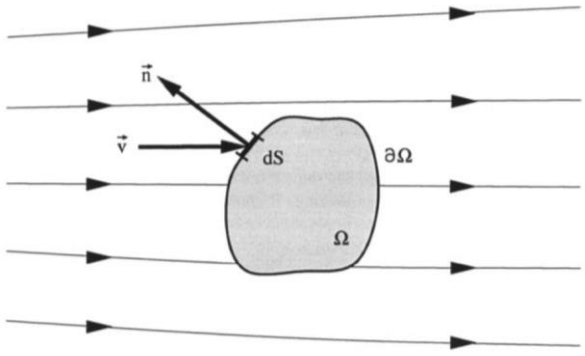

Figure 3.1 *Definition of a finite control volume (fixed in space)* (Blazek 2005).

3.2 The Continuity Equation

If we restrict our attention to single-phase fluids, the law of mass conservation expresses the fact that mass cannot be created in such a fluid system, nor it can disappear. There is also no diffusive flux contribution to the continuity equation, since for a fluid at rest, any variation of mass would imply a displacement of the fluid particles. In order to derive the continuity equation, consider the model of a finite control volume fixed in space, as sketched in **Figure 3.1** Definition of a finite

control volume (fixed in space) (Blazek 2005).***Figure 3.1***. At a point on the control surface, the flow velocity is $\vec{v}$, the unit normal vector is $\vec{n}$, and dS denotes an elemental surface area. The conserved quantity in this case is the density ρ. For the time rate of change of the total mass inside the finite volume Ω we have

$$\frac{\partial}{\partial t}\int_{\Omega} \rho \partial\Omega \qquad (1)$$

The mass flow of a fluid through some surface fixed in space equals to the product of (density) x (surface area) x (velocity component perpendicular to the surface). Therefore, the contribution from the convective flux across each surface element *dS* becomes

$$\rho(\vec{v}\cdot\vec{n})dS \qquad (2)$$

Since by convection $\vec{n}$ always points out of the control volume, we speak of inflow if the product $(\vec{v}\cdot\vec{n})$ is negative, and of outflow if it is positive and hence the mass leaves the control volume. As stated above, there are no volume or surface sources present. Thus, we can write:

$$\frac{\partial}{\partial t}\int_{\Omega} \rho \partial\Omega + \oint_{\partial\Omega} \rho(\vec{v}\cdot\vec{n})dS = 0 \qquad (3)$$

This represents the integral form of the continuity equation - the conservation law of mass.

3.3 The Momentum Equation

We may start the derivation of the momentum equation by recalling the particular form of Newton's second law which states that the variation of momentum is caused by the net force acting

on a mass element. For the momentum of an infinitesimally small portion of the control volume Ω ***Figure 3.1*** we have

$$\rho\vec{v}\partial\Omega \qquad (4)$$

The variation in time of momentum within the control volume equals

$$\frac{\partial}{\partial t}\int_{\Omega} \rho\vec{v}\partial\Omega \qquad (5)$$

Hence, the conserved quantity is here the product of the density and the velocity, i.e.,

$$\rho\vec{v} = [\rho u, \rho v, \rho w]^{\mathrm{T}} \qquad (6)$$

The convective flux tensor, which describes the transfer of momentum across the boundary of the control volume, consists in the Cartesian coordinate system of the following three components

x-component: $\rho u\vec{v}$

y-component: $\rho v\vec{v}$

z-component: $\rho w\vec{v}$

The contribution of the convective flux tensor to the conservation of momentum is then given by

$$-\oint_{\partial\Omega} \rho\,\vec{v}\,(\vec{v}\cdot\vec{n})dS \qquad (7)$$

The diffusive flux is zero since there is no diffusion of momentum possible for a fluid at rest. We can identify two kinds of forces acting on the control volume:

1. External volume or body forces, which act directly on the mass of the volume. These are for example gravitational, buoyancy, Coriolis or centrifugal forces. In some cases, there can be electromagnetic forces present as well.

2. Surface forces, which act directly on the surface of the control volume. They result from only two sources:

(a) Pressure distribution, imposed by the outside fluid surrounding the volume,

(b) Shear and normal stresses, resulting from the friction between the fluid and the surface of the volume.

From the above, we can see that the body force per unit volume, further denoted as $\rho\vec{f_e}$, corresponds to the volume sources. Thus, the contribution of the body (external) force to the momentum conservation is

$$\int_{\Omega} \rho\vec{f_e}\partial\Omega \qquad (8)$$

The surface sources consist then of two parts - of an isotropic pressure component and of a viscous stress tensor $\bar{\bar{\tau}}$, i.e.,

$$\bar{\bar{Q}}s - p\bar{\bar{I}} + \bar{\bar{\tau}} \qquad (9)$$

with $\bar{\bar{I}}$ being the unit tensor. The effect of the surface sources on the control volume is sketched in **Figure 3.2**.

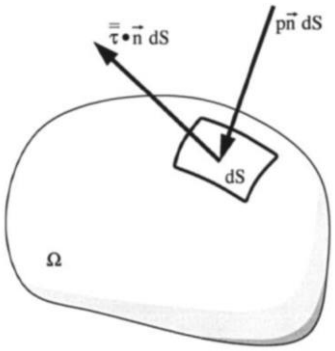

Figure 3.2 *Surface forces acting on a surface element of the control volume* (Blazek 2005).

Hence, if we now sum up all the above contributions, we finally obtain the expression:

$$\frac{\partial}{\partial t}\int_{\Omega} \rho\, \vec{v}\, \partial\Omega + \oint_{\partial\Omega} \rho\, \vec{v}\, (\vec{v}\cdot \vec{n}) dS = \int_{\Omega} \rho \vec{f_e} \partial\Omega - \oint_{\partial\Omega} \rho\, \vec{n}\, dS + \oint_{\partial\Omega} (\bar{\bar{\tau}}\cdot \vec{n}) dS \quad (10)$$

for the momentum conservation inside an arbitrary control volume Ω which is fixed in space (Blazek 2005).

3.4 Volume of Fluid Method VOF

For modelling multiphase flow in porous media, the volume-of-fluid method is used to capture the location of interfaces (Blunt et al. 2013).

In general, the VOF model is composed of a set of continuity and momentum equations, as well as a transport equation for the evolution of a phase indicator function which is used to determine the location and orientation of the interface. A common feature for all the different formulations of the VOF model is that the location and orientation of the interface are defined through a volume

fraction function. The evolution of this volume fraction function in time and space is determined by a scalar advection equation defined by:

$$\frac{D\alpha_1}{Dt} = \frac{\delta\alpha_1}{\delta t} + (v_m * \nabla)\alpha_1 = 0 \qquad (11)$$

The propagation procedure contains the calculation of the volume fraction, α_1, that represents the fractional volume of the cell occupied by fluid 1. A unit value of α_1 corresponds to a cell full of fluid 1, while a zero value indicates that the cell contains no fluid 1. Cells with α_1 values between zero and one must then contain an interface. The VOF models thus require a proper numerical advection scheme to approximate the transport of the scalar function in an accurate manner avoiding numerical diffusion. Most VOF algorithms solve the problem of updating the volume fraction field, α_1, given the fixed grid and the velocity field, v_m, using a second order explicit discretization scheme in time and a higher (second) order discretization scheme on the flux form in space (Jakobsen 2014).

3.5 Pressure-Velocity Coupling

Because of the incompressible assumption, the solution of the governing equations is complicated by the lack of an independent equation for pressure. In each of the momentum equations, fluid flow is driven by the contribution of the pressure gradients. With the additional equation provided by the continuity equation, this system of equations is self-contained; there are four equations for

four dependents, *u, v, w*, and *p*, but no independent transport equation for pressure. The implication here is that the continuity and momentum equations are all that are required to solve for the velocity and pressure fields in an incompressible flow. For such a flow, the continuity equation is a kinematic constraint on the velocity field rather than a dynamic equation. In order to link the pressure with the velocity for an incompressible flow, one possible way is to construct the pressure field so as to guarantee conservation of the continuity equation. In this section, we describe the basis of one of the most popular schemes of pressure– velocity coupling for an incompressible flow. It belongs to the class of iterative methods that is embodied in a scheme called SIMPLE, where the acronym stands for Semi-Implicit Method for Pressure-Linkage Equations. The SIMPLE scheme was developed for practical engineering solutions by Patankar and Spalding (Patankar and Spalding 1972). In the SIMPLE scheme, a guessed pressure field is used to solve the momentum equations. A pressure correction equation, deduced from the continuity equation, is then solved to obtain a pressure correction field, which in turn is used to update the velocity and pressure fields. These guessed fields are progressively improved through the iteration process until convergence is achieved for the velocity and pressure fields (Tu, Yeoh, and Liu 2009).

3.6 PISO, SIMPLE and PIMPLE Algorithms in Openfoam

Most fluid dynamics solver applications in OpenFOAM use either the pressure-implicit split-operator (PISO), the semi-implicit method for pressure-linked equations (SIMPLE) algorithms, or a combined PIMPLE algorithm. These algorithms are iterative procedures for coupling equations

for momentum and mass conservation, PISO and PIMPLE being used for transient problems and SIMPLE for steady-state.

While all the algorithms solve the same governing equations (albeit in different forms), the algorithms principally differ in how they loop over the equations (CFD Direct 2018).

4 CHAPTER 4: MODEL SETUP

When two (or more) immiscible fluids share the same pore space, their spatial distribution is governed by capillary phenomena. This refers to the effects of the interfacial tension that exists in the molecular layers that make up the border between two fluids, or between a fluid and the wall, and the resulting capacity of a fluid to wet the solid. It is therefore clear that the morphology of the pore space is the element that gives structure to the spatial distribution of the fluid phases within it, and everything that ensues for the transport and transfer phenomena (Al-Gharbi and Blunt 2005).

In this chapter, variations in pore events in a immiscible drainage process in eight different patterns are shown, two cases in an homogeneous porous media (1 mPas and 10 mPas, three cases with a vertical heterogeneity (1 mPas, 10 mPas and wider heterogeneity), and three with an horizontal heterogeneity (1 mPas, 10 mPas and wider heterogeneity) all in a water wet porous media with a porous plate at the end. Graphs of pressure and fluid saturation versus time will be presented in this chapter.

4.1 Semi-permeable membrane displacement processes simulation

This thesis shows a semi-permeable membrane displacement process simulation. As mentioned in chapter 3, porous plate method is time consuming, reason why is not the most common method to measure capillary pressure. However, been a 2D simulation work, time is not an issue and has many advantages, such as there is no chance of a mistake in maintaining a good capillarity contact between the plate and the core and no weight is needed to maintain immobile the plate.

4.2 Grid setup

A pattern image was obtained and processed in Simpleware software and exported as a grid ready to use in OpenFoam. After the grid is obtained, it is imported to OpenFOAM to adequate it to the desired size, to rename the boundaries and to adjust it completely to the desired mesh. To have a pore size simulation the mesh size was established to be 0.0020 x 0.00111m x1x10^{-5} m3.

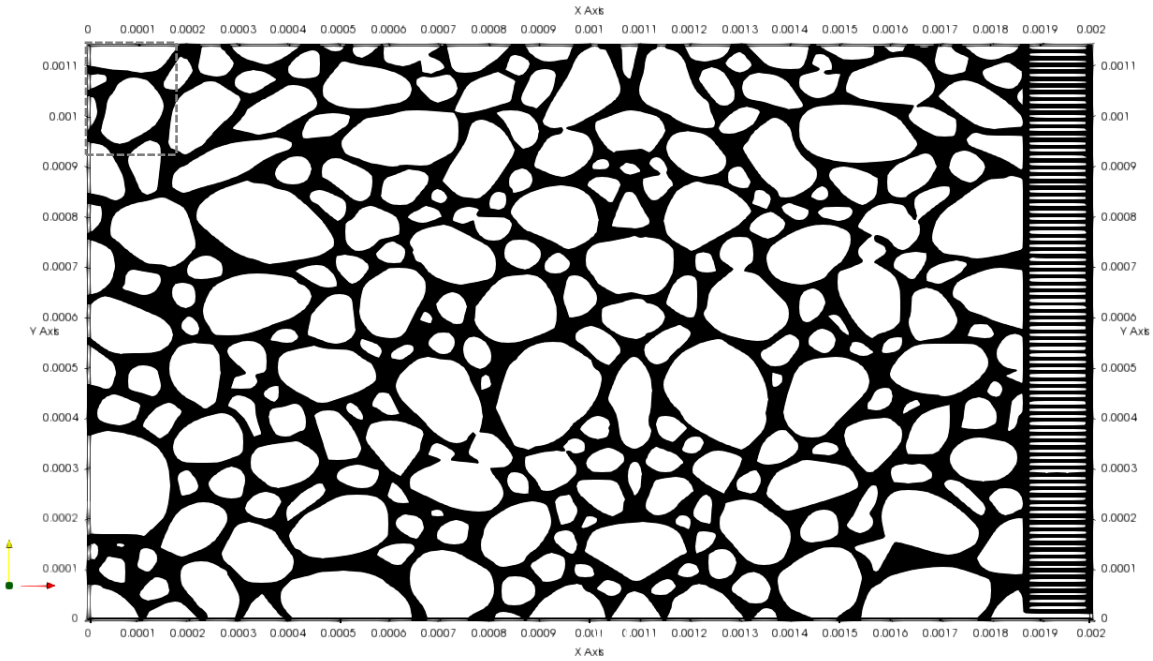

Figure 4.1 *Mesh Result for a Synthetic Image of a Sandstone Pattern with a porous plate at the end.*

To investigate differences in flow pattern, pressure behavior, final recovery, etc. five different patterns where created ass it can be seen in the next images:

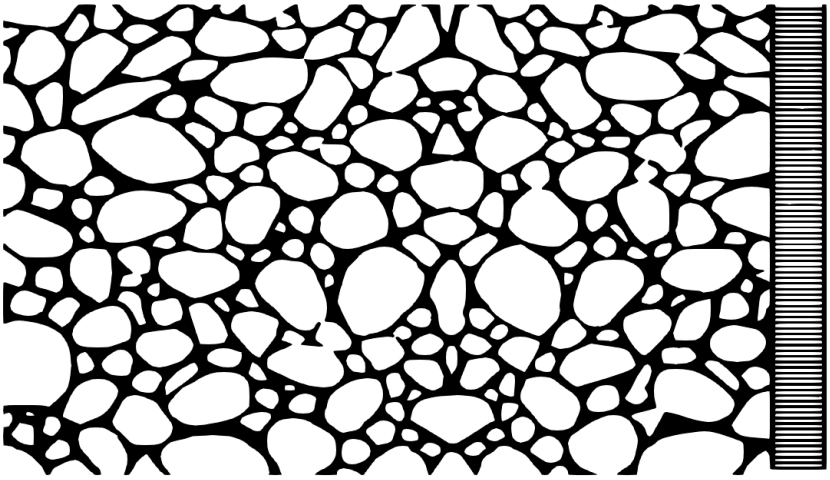

a) No discontinuity porous media.

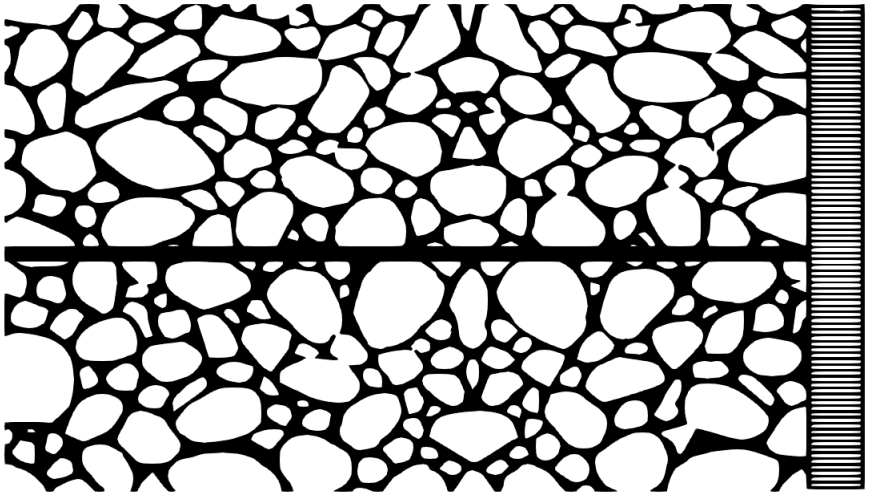

b) Thinner horizontal discontinuity. A thin horizontal discontinuity was introduced to the porous media in order to investigate its effect during drainage process.

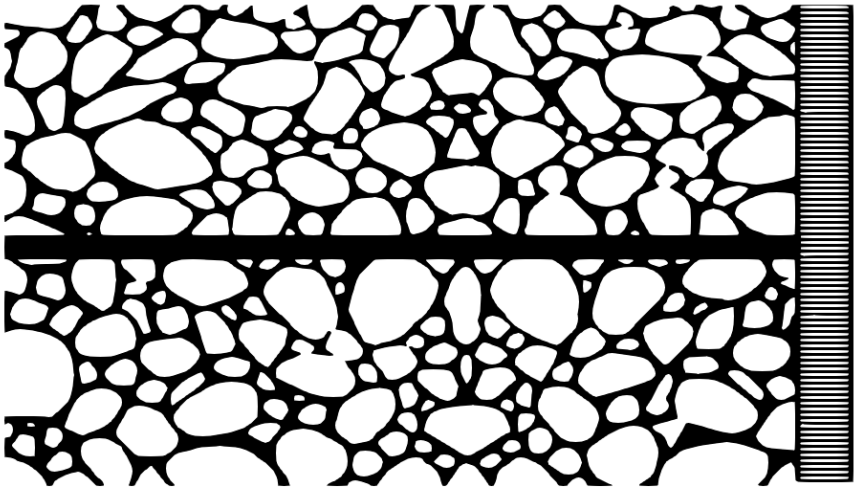

c) Thicker-horizontal discontinuity. A thick horizontal discontinuity was introduced to the porous media in order to investigate its effect during drainage process

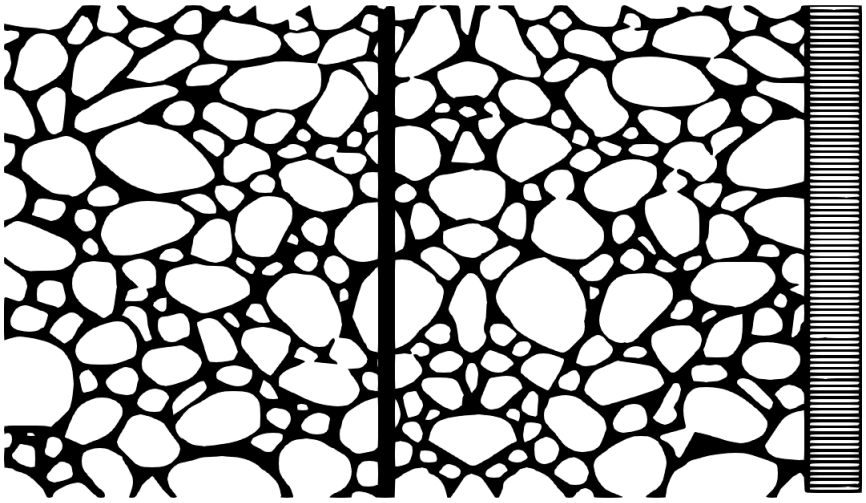

d) Vertical discontinuity. A thin vertical discontinuity was introduced to the porous media in order to investigate its effect during drainage process.

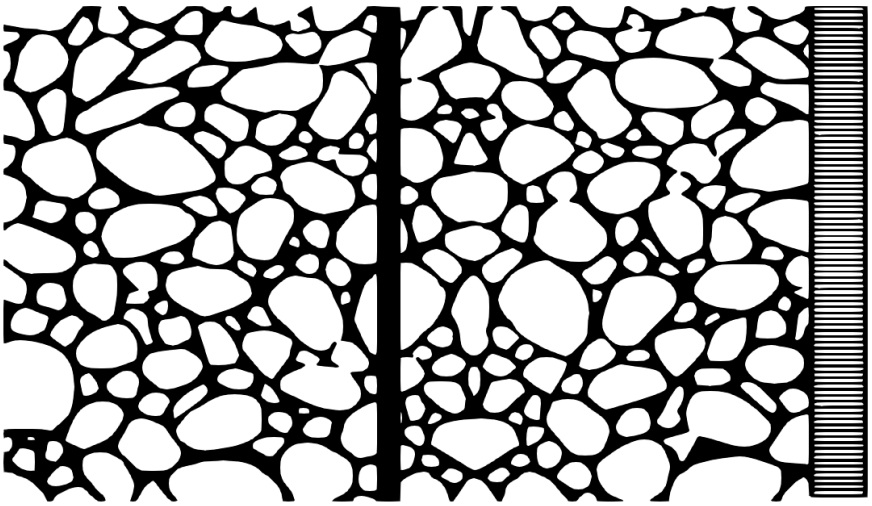

e) Thicker-vertical discontinuity. A thin vertical discontinuity was introduced to the porous media in order to investigate its effect during drainage process.

Figure 4.2 *Demonstration of discontinuities (heterogeneities) in the pore pattern. Four different discontinuities are introduced into the porous pattern to analyze its effect*

4.3 Model setup

Eight different cases of drainage where put it to run with the following characteristics:

No Fracture $\begin{cases} Nofracture\ \mu_{nw} = 0.001\ Pa \cdot s = 1\ mPas \\ No\ fracture\ \mu_{nw} = 0.01\ Pa \cdot s = 10\ mPas \end{cases}$

Horizontal Fracture $\begin{cases} Small\ fracture\ and\ \mu_{nw} = 0.001\ Pa \cdot s = 1\ mPas \\ Wider\ fracture\ and\ \mu_{nw} = 0.001\ Pa \cdot s = 1\ mPas \\ Wider\ fracture\ and\ \mu_{nw} = 0.01\ Pa \cdot s = 10\ mPas \end{cases}$

Vertical Fracture $\begin{cases} Small\ fracture\ and\ \mu_{nw} = 0.001\ Pa \cdot s = 1\ mPas \\ Wider\ fracture\ and\ \mu_{nw} = 0.001\ Pa \cdot s = 1\ mPas \\ Wider\ fracture\ and\ \mu_{nw} = 0.01\ Pa \cdot s = 10\ mPas \end{cases}$

U = 1x10-4 $\frac{m}{s}$

$P = f\ (U)$

$\nu_w = 1 \times 10^{-6}\ \frac{m^2}{s}$

$\rho_w = 1000\ \frac{kg}{m^3}$

$\mu_w = \rho_w\ \cdot\ \nu_w =\ 1 \times 10^{-6}\ \frac{m^2}{s} \cdot\ 1000\ \frac{kg}{m^3} = 0.001\ \frac{kg}{m^3} = 1\ mPas$

$\nu_{nw} = 1 \times 10^{-6}\ or\ 1 \times 10^{-5}\ \frac{m^2}{s}$

$\rho_{nw} = 1000\ \frac{kg}{m^3}$

$\mu_{nw} = 1\ mPas\ or\ 10\ mPas$

$\sigma = 0.045$

5 CHAPTER 5: RESULTS AND DISCUSSION

In this section, simulation results will be presented. The process is drainage, an immiscible and incompressible displacement, in a homogeneous porous medium depicted as a rectangular image of 0.002 x 0.0011 x $1x10^{-5}$ m^3, containing 128,595 cells with a porous plate at the end of the porous medium preventing (capillary barrier) oil flow (non-wetting fluid), but allowing water flow. The pore sizes of the porous disk should be small enough to prevent penetration of the displacing fluid until the water saturation in the core has reached its irreducible value. The pore openings control the matrix pressure, *P*, at which pores empty, whereas the wider pore bodies control the pressures at which pore fills.

In this dynamic network a specified inflow rate of oil of a Darcy velocity of $1x10^{-4}$m/s is imposed at the inlet (left side), and the subsequent transient pressure response and the associated interface positions are calculated. At the outlet (right side), atmospheric pressure is imposed. The upper and lower walls are defined as no-flow boundaries. The density of oil and water were kept the same, 1000kg/m^3, in order to eliminate gravity effects, interfacial tension $\sigma = 0.045\ N/m$, water viscosity was set to μ_w=1mPa*s=1cP, and oil μ_o=10mPa*s = 10cP for some cases and μ_o=1mPa*s = 1cP for other cases. The medium is water-wet, with a zero-contact angle at the walls, θ=0°.

Porosity was calculated with the void volume divided by the total volume, $\phi = \frac{V_T}{V_{Void}} = \frac{7\text{x}10-12\ \text{m}3}{2.2\text{x}10-11\ \text{m}3} * 100 = 31.82\%$.

The ratio of viscous to capillary forces is, $Ca = \frac{\mu V}{\sigma} = \frac{\mu V}{\sigma} = 2x10^{-6} and\ 2x10^{-5}$, viscous forces become significant at the pore scale only when *Ca* is in the range of 10^{-4} or higher (Tsakiroglou, Avraam, and Payatakes 2004). In **Figure 5.1** A pattern image of a reservoir sandstone of size 0.002m x 0.001m. shows the pore space and the initial conditions.

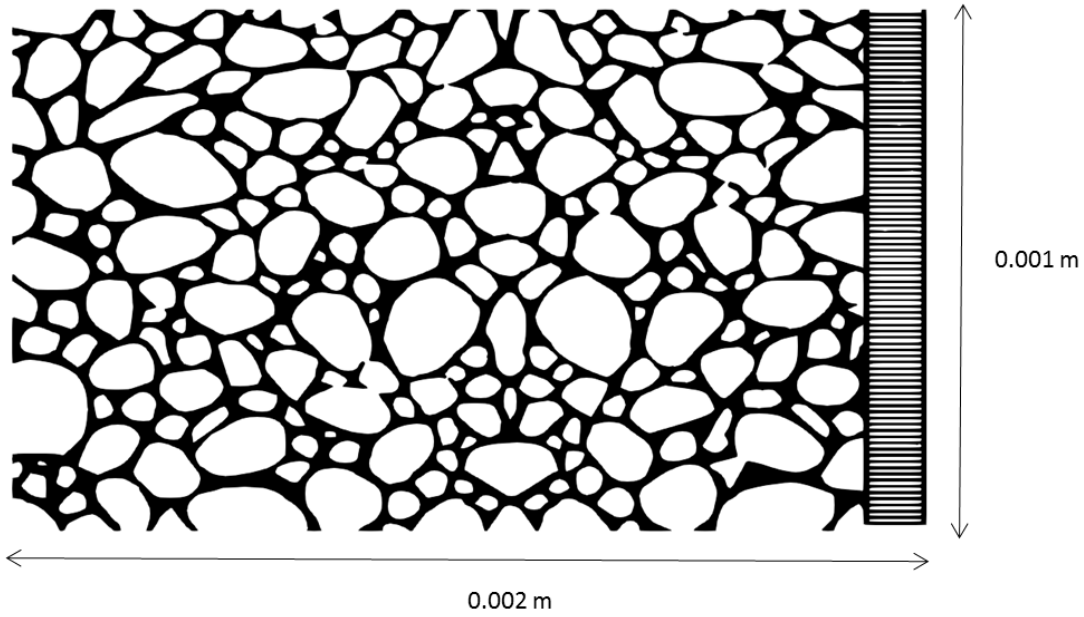

Figure 5.1 *A pattern image of a reservoir sandstone of size 0.002m x 0.001m.*

5.1 Drainage in a homogeneous porous medium, 1mPas

Initially, the system is completely saturated with water (the wetting fluid). The invading fluid is oil (non-wetting fluid) which displaces water from the inlet side with a constant injection rate. To achieve displacement, the pressure in the oil must increase above atmospheric which is the pressure condition in the outlet.

The oil advance takes place in the direction of the decreasing pore diameter. As the pressure is increased, further penetration of the oil phase into the porous medium is achieved until the local minimum pore radius is reached. The capillary pressure at the throat exceeds the equilibrium value in the subsequent expanding portion of the pore. Therefore, the penetration into the expanding portion of the pore occurs in a non-equilibrium manner. In other words, there is a finite net force present throughout, which drives the wetting phase out. Non-equilibrium penetration will continue until the meniscus reaches a throat that is narrower than the previous one. At that point the applied capillary pressure must be increased further to penetrate this throat, and so forth. The process in which the nonwetting phase displaces the wetting phase is usually called "drainage," "desaturation," or "de-wetting" (Dullien 1992).

Pressure mobilization-breakup occurs at an average patch pressure of 2,685Pa, which gives a pore size of 43μm. At early times (t=0.158s) oil advances quicker through the widest pores which are approximately in the center of the inlet.

While the medium is drained, we can see individual pore-scale displacements in the form of Haines jumps. These jumps often happen in cascades, which is explained as sequential filling of pores

with lower entry capillary pressure than the first pore of the cascade. Haines jumps in individual pores have been found to happen regardless of the externally imposed capillary number (Bultreys et al. 2015). These can be seen at times 0.348, 0.418, 0.568, 0.778, 0.918s and pressures equal to 6,434, 5,471, 4,404, 4,626 and 4,510Pa. Jumps occur when oil passes from a lower entry capillary pressure than the first pore. ***Figure 5.2***.

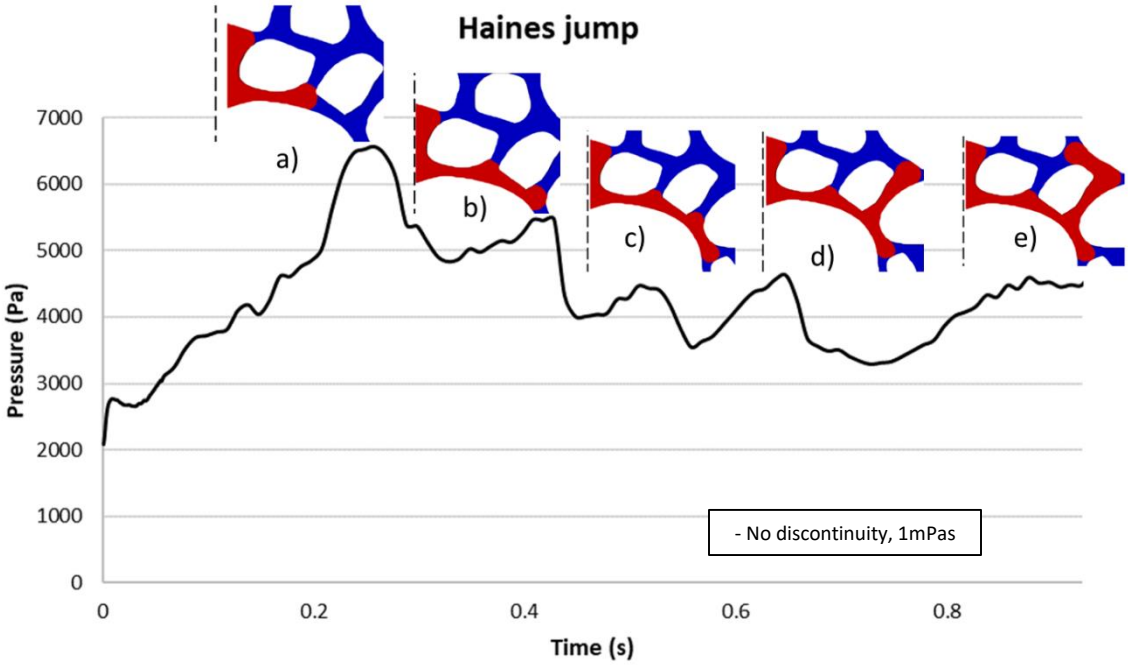

Figure 5.2 *A sequential filling of pores where oil passes from a pore neck with lower entry capillary pressure than the first pore, causing Haines Jumps. a) t = 0.348s, P=6,434Pa. b) t = 0.418s, P=5,471Pa. c) t = 0.568s, P=4,404Pa. d) t = 0.778s, P=4,626Pa. e) t= 0.918s, P= 4,510Pa.*

The next pore event process that can be measured quantitatively is seen from *t*=1.628s to 1.658s when oil emerges from a water-wet constriction into a water-filled pore. The interface forces are

such that a leading portion of the oil may separate into a droplet (snap-off). Theory indicates that for a given shape of constriction, there is a minimum size to the protruding portion of the oil that permits snap-off. The disconnected oil is in the form of discrete oil blobs, named ganglia, which are trapped in the pores of the reservoir. As the capillary pressure of the connected oil is larger than that of the disconnected phase, with further oil injection it can reconnect (Roof 1970), see ***Figure 5.3.***

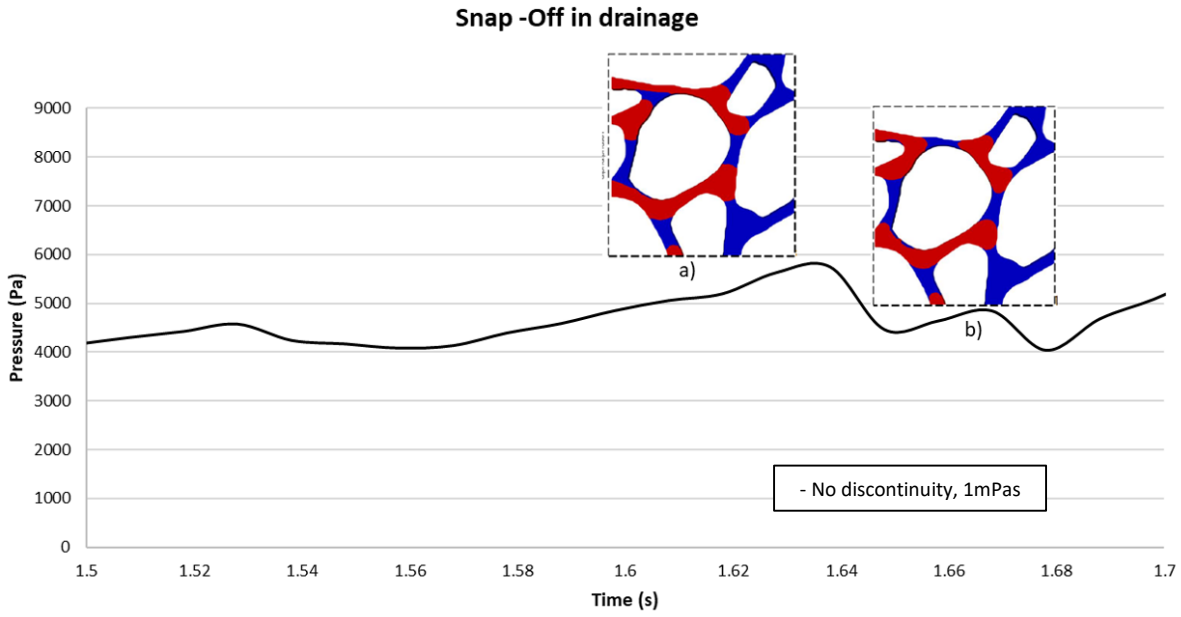

Figure 5.3 Snap –off event. a) Shows the throat pore filled with oil before the snap off occurs, P=5,743Pa. which is not enough to displace oil. b) Shows the oil ganglion disconnection caused by the snap-off event, P=4,462Pa oil disconnection occurs and pressure decrease.

Drainage continues until the irreducible water saturation is reached (S_{wir}). During this process, oil advances through the porous space and at t=3.478s three main oil stream paths can be noticed. The first oil stream path is located in the left upper corner in the porous medium. The second one

is located in the middle of the porous medium and the third one in the lower part of the medium. However, at *t*=5.808s when the two upper oil stream paths are advancing approximately in the middle of the porous medium they collide and form one main oil stream making it the strongest oil path in the medium and the third one remains with less strength until t=8.358s, when the connection between the oil path and the inlet is broken, causing an oil bank formation because that oil accumulation is not further reconnected with the inlet or any other oil stream around. -see **Figure 5.4.**

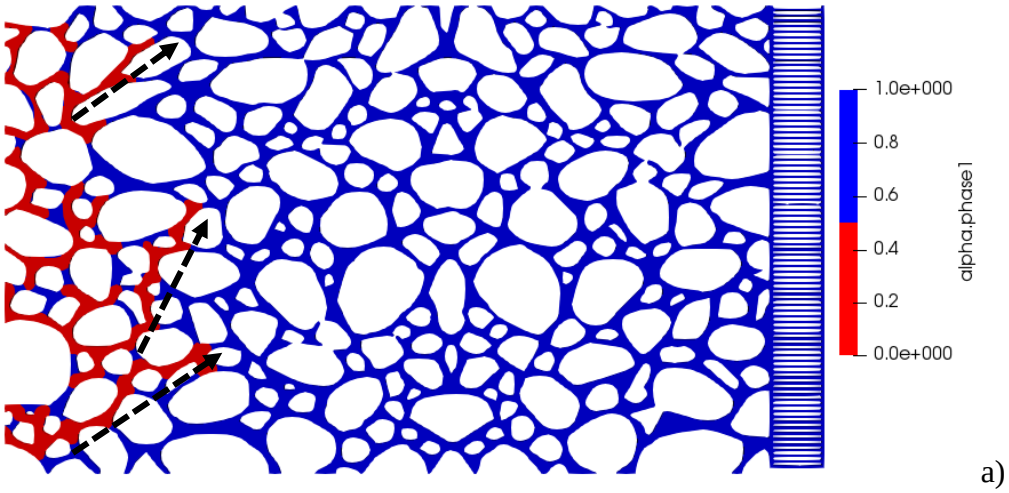

a)

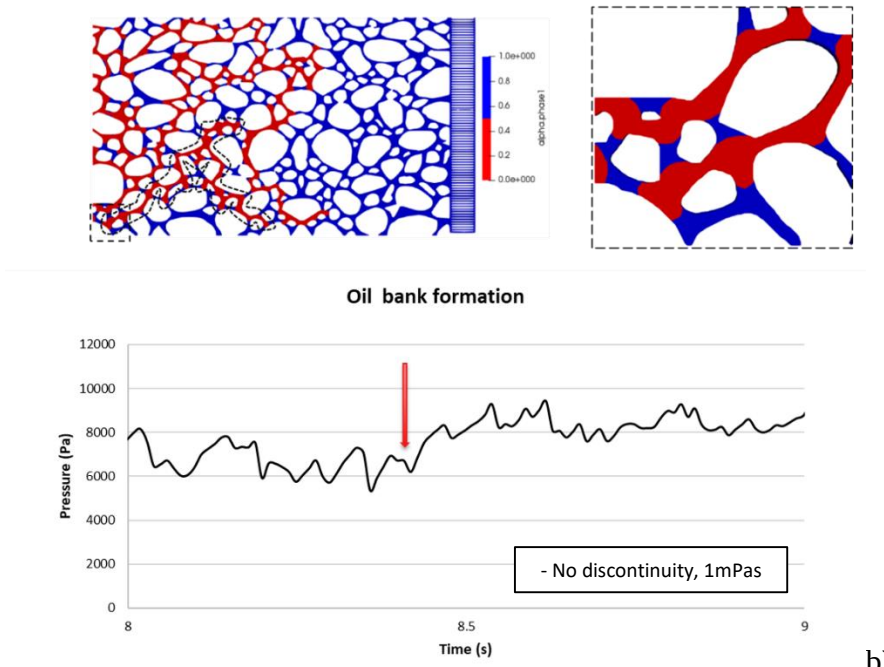

b)

Figure 5.4 *a) Three arrows are pointing the three main oil stream paths, where most of the oil is heading, b) t=3.478s, P=6,344Pa. The oil stream path located in the lower part is driven only by the lowest left throat, a snap-off occurs and disconnects oil. This snap-off causes the disconnection of the lower oil stream, leaving a considerable big oil ganglion trapped in the media.*

At the end of the drainage process, (t=14.7s, P=12,000Pa) oil banks and oil ganglia are stranded in the medium, and irreducible water saturation is reached (S_{wir}=0.42). No volume of oil has entered yet into the porous plate. This means that the pore sizes of the porous disk accomplished the task of preventing penetration of the displacing fluid (oil) until the water saturation in the porous media reached its irreducible value, but a film of oil is placed in front of the porous plate as can be seen in **Figure 5.5.**

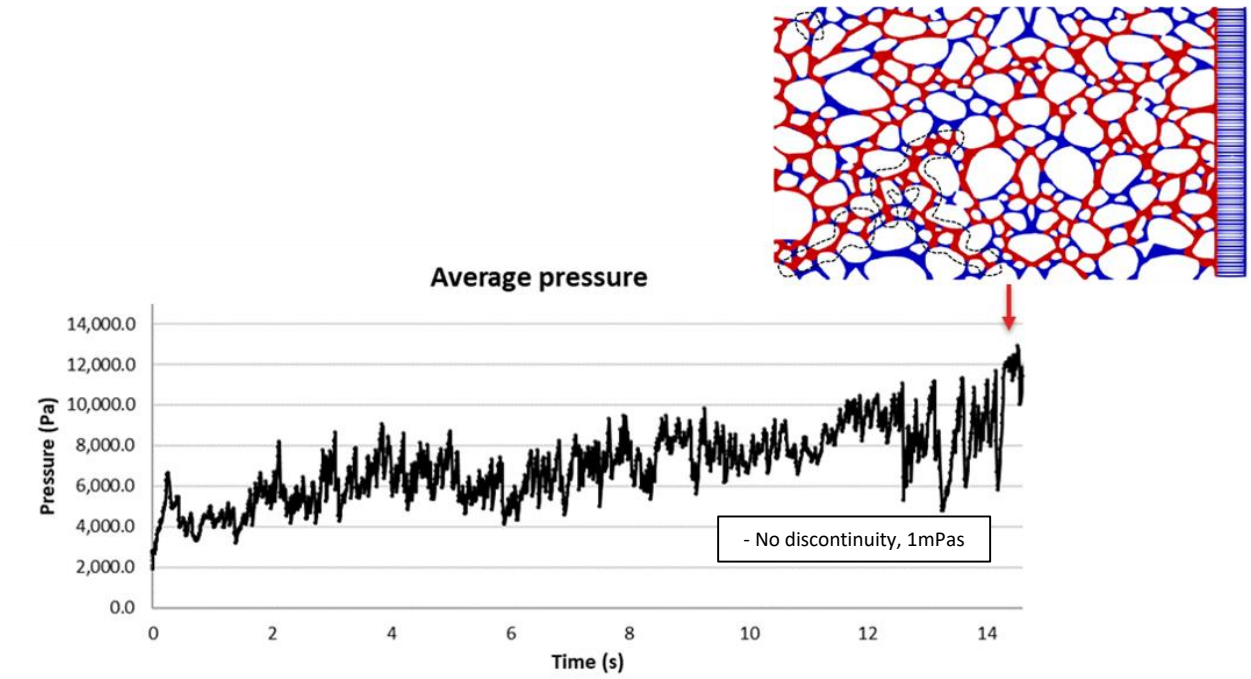

Figure 5.5 *At the end of the drainage process, initial oil saturation is established, and the residual water saturation is reached, in the black circles we can see oil ganglia, and oil clustered stranded into the porous medium, it can be noticed also that no volume of oil has passed through the porous plate. (t=14.7s, P=12,000Pa)*

Finally, we can observe how pressure increases until its maximum value. In that stage, oil is placed between the porous plate and the porous media, then oil starts crossing the porous plate ***¡Error! No se encuentra el origen de la referencia.***. Finally, at *t*=15.098s oil pressure exceeds the porous plate breakthrough pressure. This is the highest point in pressure in the fifth stage in the graph, the next jumps are similar events, oil goes through the porous plate, see ***Figure 5.6.***

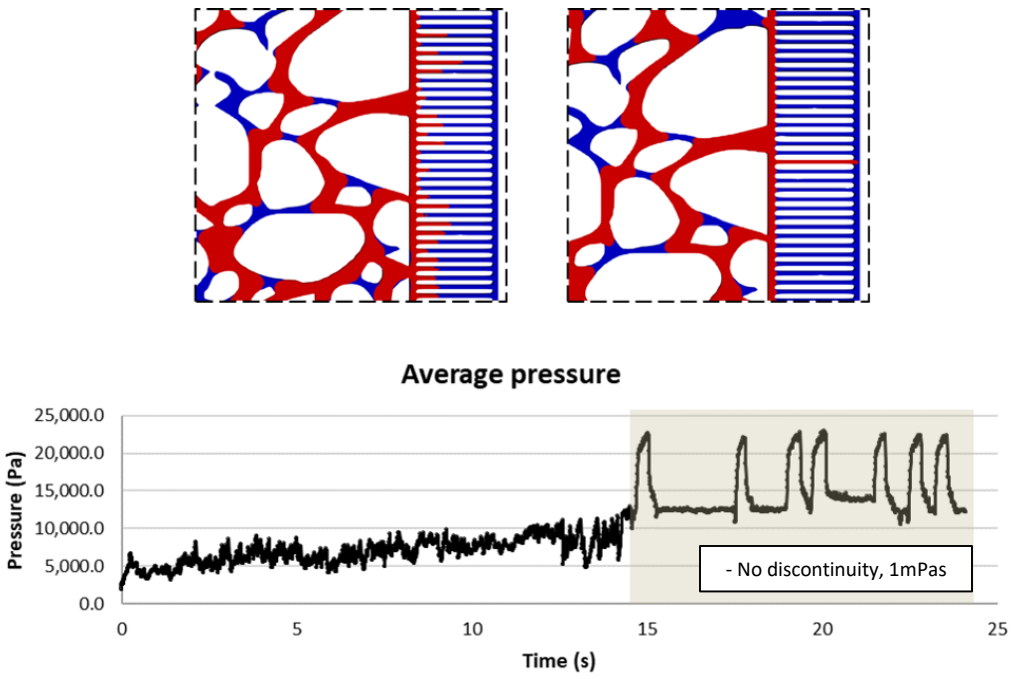

Figure 5.6 *At the end of the drainage process oil starts crossing the porous plate.*

In the final view of drainage simulation, we can observe three oil ganglia. According to Lenormand's (Lenormand 1990) phase diagram, all cases simulated in this thesis are in the capillary fingering regime (low capillary number of injection (C<1) and ($\log_{10}(M)$ higher and lower than 0), where pore-by-pore capillary pressure drops dominate and the non wetting fluid will tend to invade the pores that show the lower capillary resistivity (the biggest ones). During capillary finger regime, although the advancing front is rather flat, return front of the nonwetting phase and trapping of the wetting fluid (blobs formation) must be expected, see **Figure 5.7**.

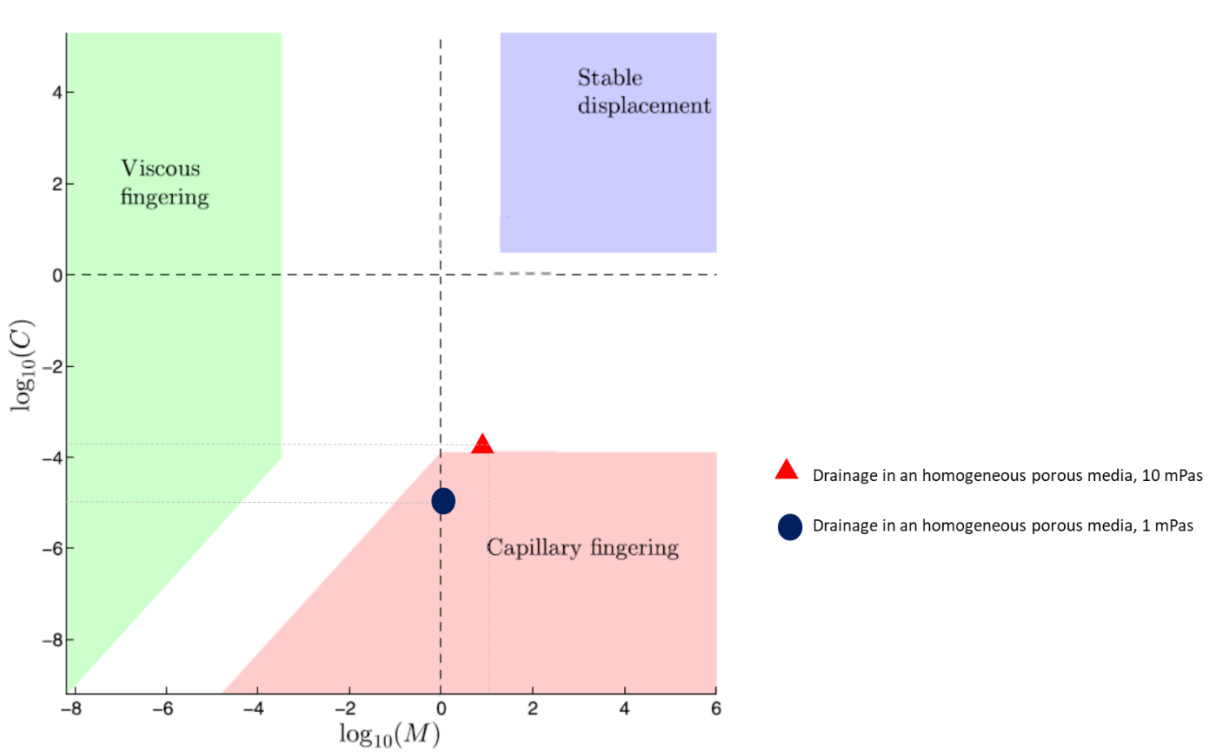

Figure 5.7 *Lenormand's phase diagram. Viscous fingering (light Green), capillary fingering (light red), and stable displacement front (Deep blue). Dark blue circle: Drainage in a homogeneous porous media 1mPas [log10 (M)=0 and log10 (C)=-5.7]. Red triangle: Drainage in a homogeneous porous media, 10mPas [log10 (M)=1 and log10 (C)=-4.7].*

A graph of capillary pressure vs. oil saturation during drainage was built. Pressure increases because the filling sequence depends on the capillary pressure of the system. The first pore to be drained is the biggest pore, where pressure, as expected, has the lowest value. Lower pressure allows oil to find the least resistance front. Then oil advance takes place in the direction of decreasing pore diameter and as pores decrease, pressure increase until the minimum pore radius

has reached, see

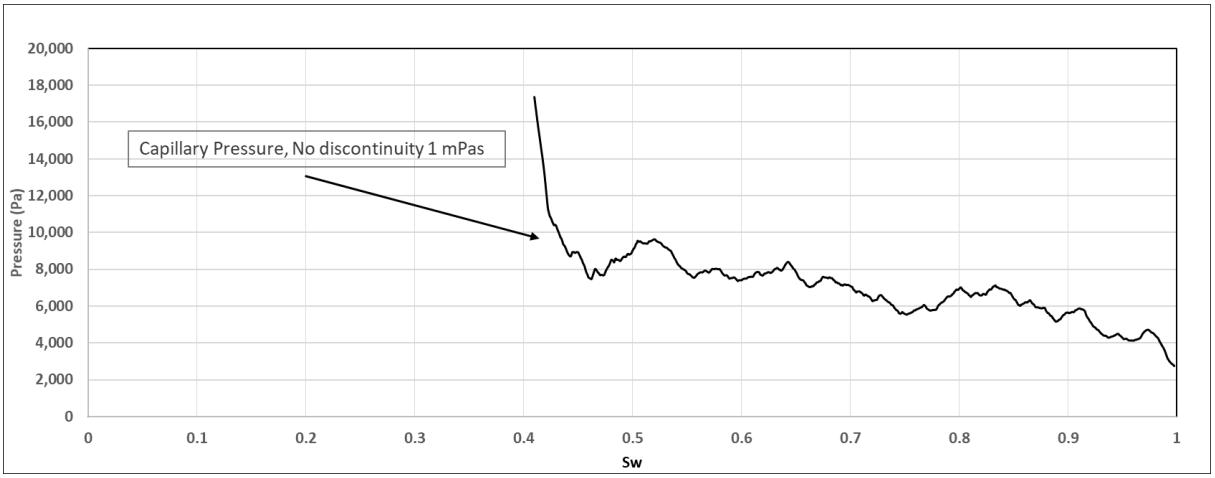

***Figure* 5.8**.

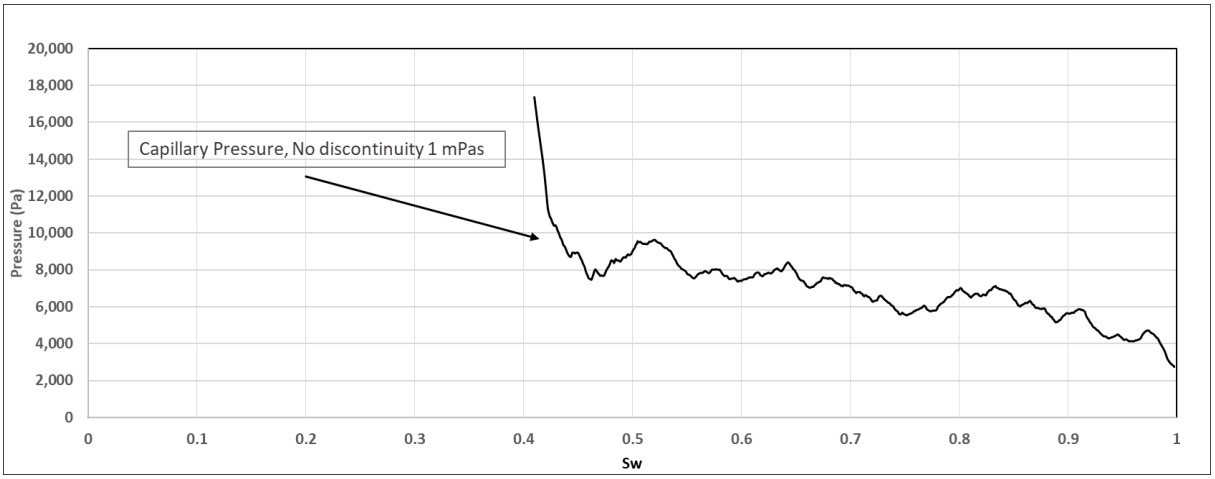

Figure 5.8 *Capillary pressure during drainage. When oil crosses the porous plate* S_{wir}*=0.04, P=22,135Pa. Oil entrance pressure is given at P=2014Pa. Water saturation decreases from 1 to 0.4 when the porous plate is reached.*

A graph of oil and water saturation versus time with a slope of 0.0394 ($.s^{-1}$). It can be observed that oil augments with time until no change in oil saturation is noticed. At the beginning, oil saturation is zero S_{oi}=0 and initial oil saturation at the end of the drainage process is S_{oi}=0.59. **Figure 5.9** displays oil saturation behavoir.

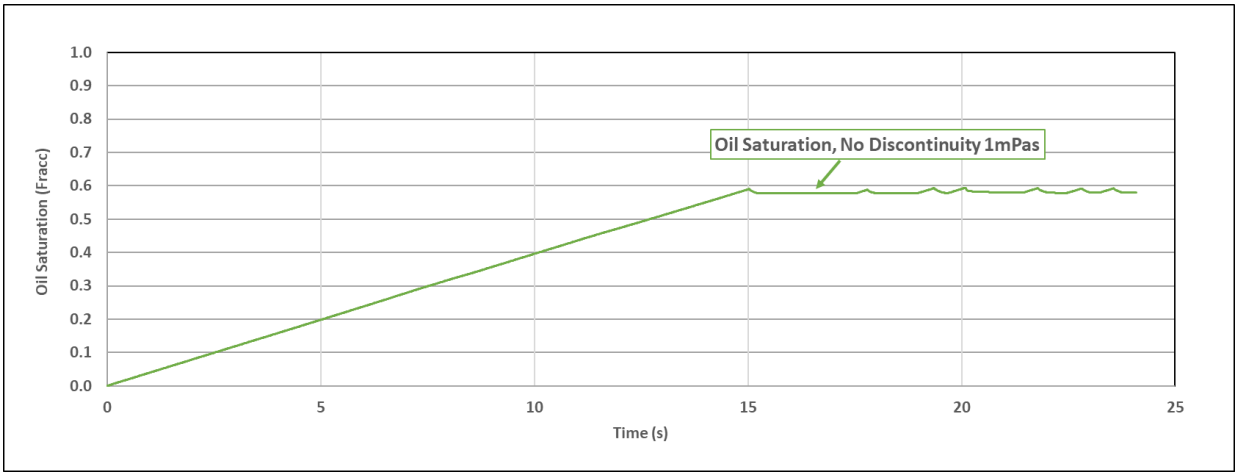

Figure 5.9 *Oil saturation vs. time. Case: Homogeneous porous medium, 1mPas.*

The exact opposite behavior can be seen in water saturation. At the start, water saturation is equal to 1, the medium being fully saturated with water. As time goes on, water saturation is reduced until the irreducible water saturation is reached, in this case the S_{wir}=0.42. ***Figure 5.10*** illustrates water saturation behaviour during drainage.

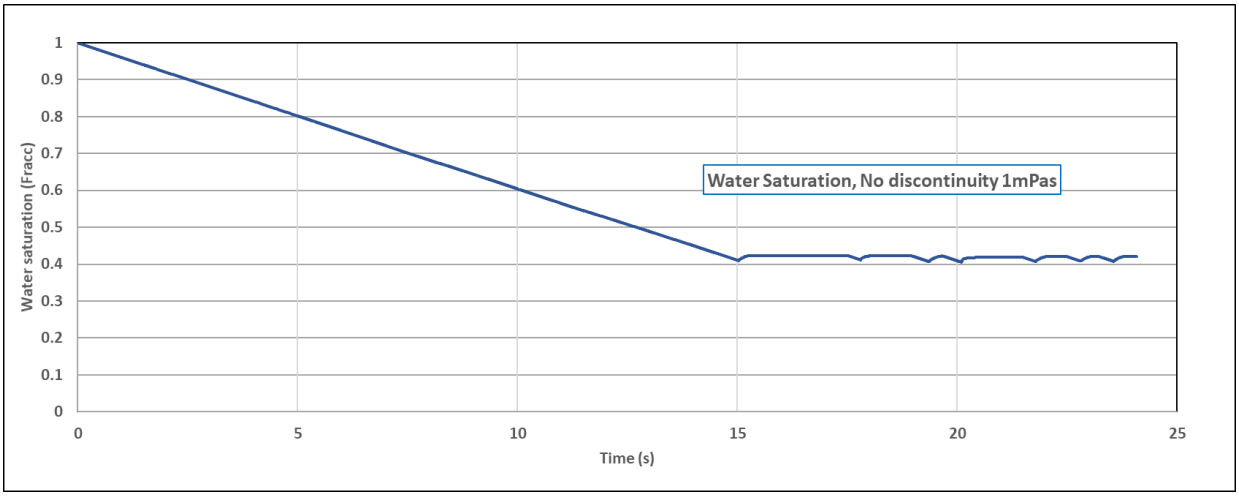

Figure 5.10 *Water saturation vs. time. Case: Homogeneous porous media, 1 cP.*

5.2 Drainage in an homogeneous porous media, 10 $mPas$.

A second case where the non-wetting fluid viscosity increased from $1mPas$ to $10mPas$ in the first porous medium pattern was run. A more viscous fluid implies higher friction between the fluid and the pore walls resulting in higher pressures needed to displace oil into the porous media, higher capillary pressures invades smaller pores, resulting in higher oil saturations at the end of the drainage.

As in the previous case, almost the same pore events can be seen along the simulation. Oil adhesion can be seen due to higher viscosity in the non-wetting fluid. In order to demonstrate the viscosity effect on drainage, one porous event is going to be mentioned. First ganglia coalescence is seen from 1.11 s (5,342 Pa) to 01.12 s (3,744 Pa), a pore is filled when two oil ganglia from different directions filled the pore. As observed in the next figure, oil adhesion is observed and is pointed

with black arrows, it can be appreciated that when oil coalescence takes place, oil adheres to the lower grains, which at the end results in higher capillary pressures needed to displace oil throughout porous media, hence, resulting in more water drained, see ***Figure 5.11***.

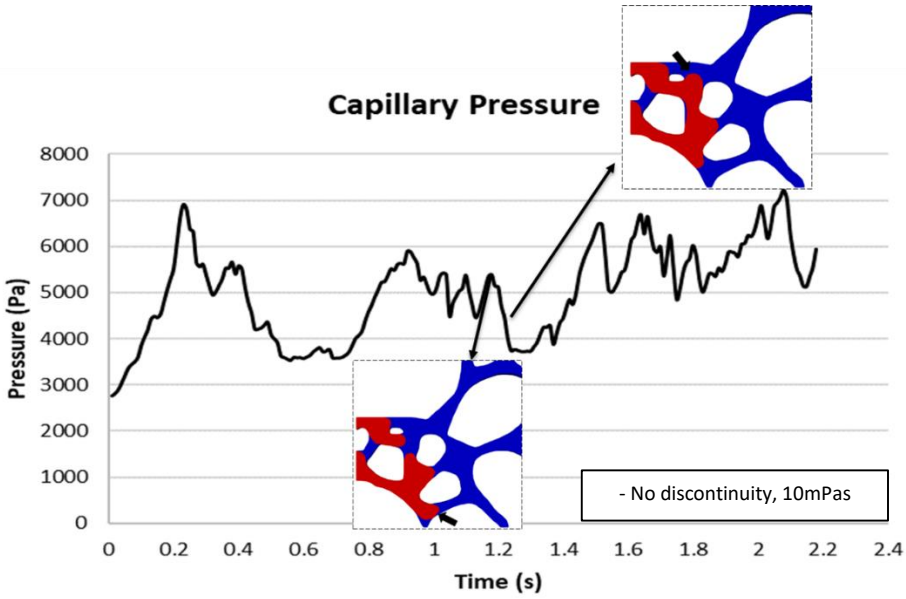

Figure 5.11 *At the bottom two oil ganglia coming from different directions to the same pore (t=1.11, P=5,342 Pa). At the top, two oil ganglia filling the same pore (t=1.13, P=3,744 Pa). At the pore space ganglia coalescence can be appreciated if two individual ganglia come into a pore from different directions*

At the end of the process oil reaches the porous plate at t=15.61s, where we can see oil covering the left side of the porous plate, no more water can flow anymore and any oil ganglia remains trapped.

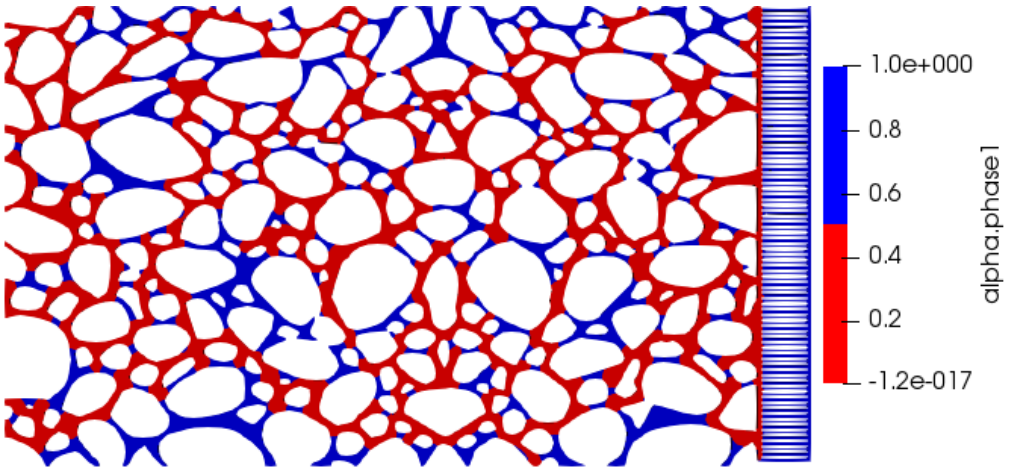

Figure 5.12 *t=12.6 s. End of drainage process, no more water is flowing through the porous plate and a film of oil is place in front of the porous plate.*

Comparing the cases “drainage in a homogeneous porous media, 1 mPas” and the case “drainage in a homogeneous porous media, 10 mPas”, most of the pore events can be seen in the same order, in the same zones. As we observed during this case, oil adhesion is higher for this case, hence higher capillary pressures are needed to push oil inside the porous media.

Due to higher viscosity generates higher friction between the fluid and the pore walls resulting higher pressures to displace the oil into the porous media, higher capillary pressures invades smaller pores, resulting in higher oil saturations at the end of the drainage. Drainage occurs faster in the case “drainage in a homogeneous porous media, 1 mPas” than the case “drainage in an homogeneous porous media, 10 mPas”.

In the next graph a Capillary Pressure comparison between the cases drainage in a homogeneous porous media, 1 mPas” and the case “drainage in an homogeneous porous media, 10 mPas” is

done, where we can appreciate higher capillary pressures for the case “drainage in an homogeneous porous media, 10 mPas” and lower $S_{wir,}$=0.38, see ***Figure 5.13***

As it was stated in previous case, ***Figure 5.7*** Lenormand’s phase diagram, the more viscous non-wetting phase case has more stability during drainage.

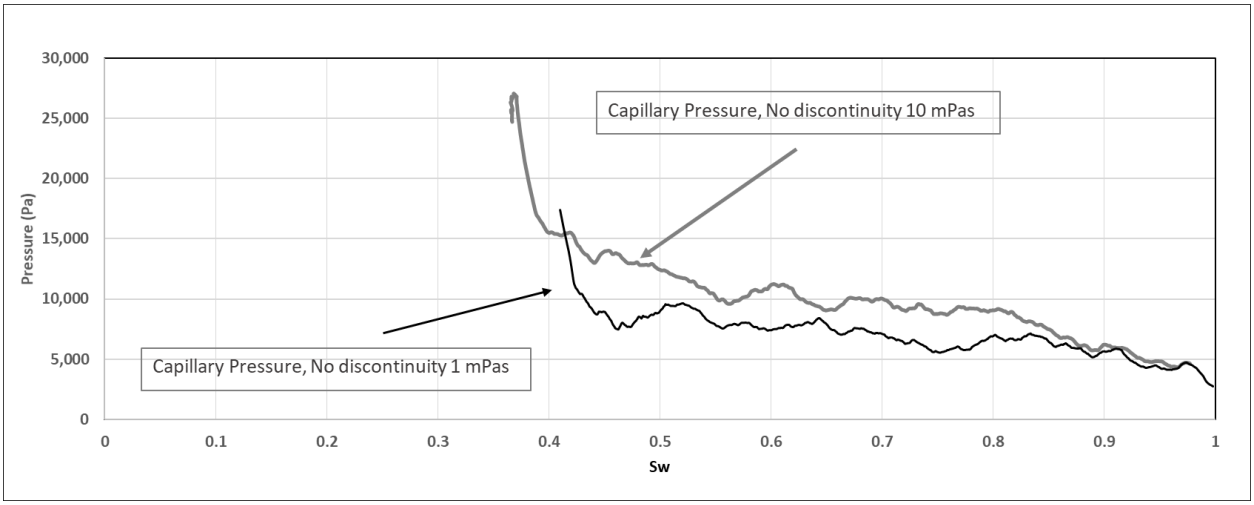

Figure 5.13 *Capillary pressure, comparison. In the graph we observe that pressure average is higher for the case “drainage in an homogeneous porous media, 10 mPas” than the case “ drainage in an homogeneous porous media, 1 mPas”, and drainage process is faster in the case “ drainage in an homogeneous porous media, 1 mPas” than the case “drainage in an homogeneous porous media, 10 mPas”.*

A graph of oil and water saturation versus time was done. In the first graph, we can notice that oil augments with time until no change in oil saturation is notice, at the beginning, the oil saturation is zero S_{oi}=0 and the oil saturation reached at the end of the drainage process is S_{oi}=0.62. ***Figure 5.14*** displays the oil saturation behavoir.

Comparing oil saturation in both cases, this case with higher viscosity ($10\ mPas$) has more oil saturation at the end of the process (S_{oi}=0.62) due to viscous forces are bigger for the higher oil viscosity, overall displacement pressure is higher due to more friction between the fluid and the pore walls, hence pores with smaller radius can be invaded resulting in slightly higher oil saturation.

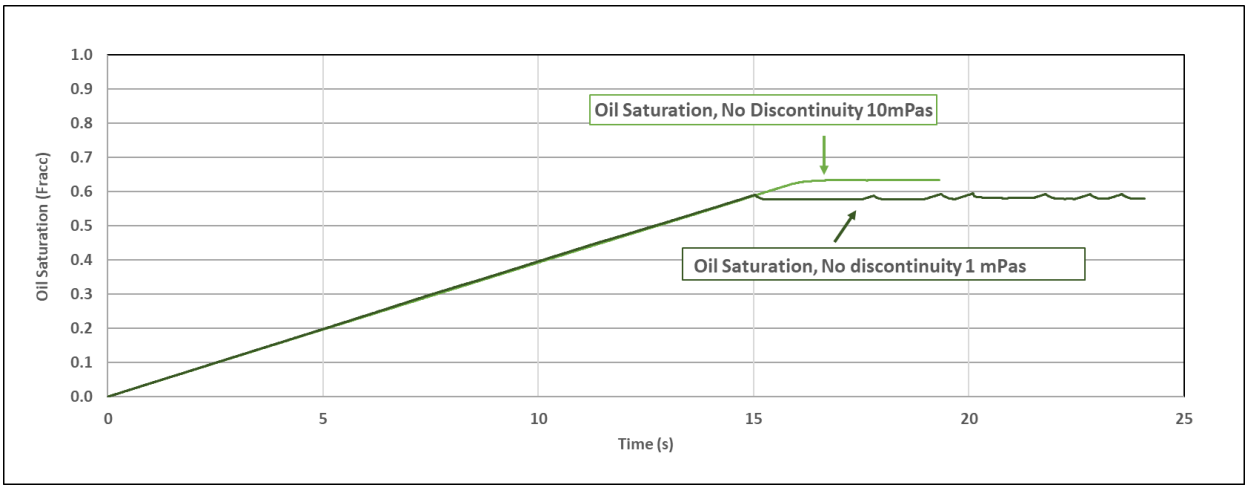

Figure 5.14 *Oil saturation vs time. Case: Homogeneous porous media, 10 mPas. Comparing oil saturation in both cases, this case with higher viscosity (10 mPas) has more oil saturation at the end of the process (S_{oi}=0.62) due to viscous forces are bigger.*

Opposite behavior can be seen in water saturation. At the start, water saturation is equal to 1, the media is fully saturated with water. As time goes on, oil saturation is reduced until the irreducible water saturation is reach, in this case the S_{wir}=0.38. ***Figure 5.15*** illustrates the water saturation behaviour during drainage.

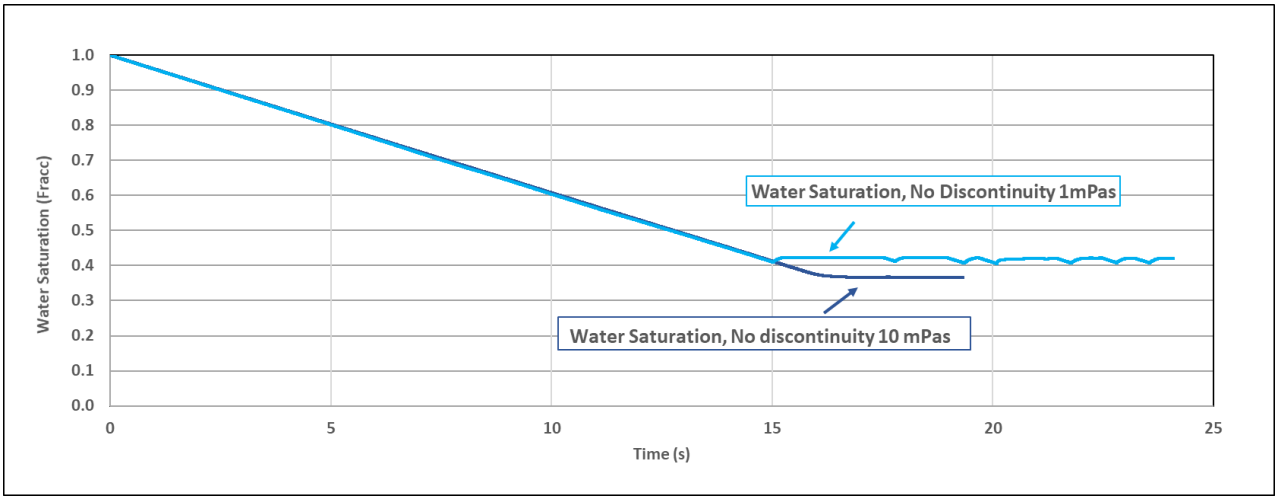

Figure 5.15 *Water saturation vs time. Case: "Homogeneous porous media, 10 mPa". Oil saturation is reduced until the irreducible water saturation is reach, in this case the* S_{wir}*=0.38.*

5.3 Drainage in a vertical discontinuity. 1mPas.

A test adding a vertical discontinuity with a width of 40 μm into the porous media was done to investigate differences in capillary pressures, oil saturation and drainage time, see ***Figure 5.16***.

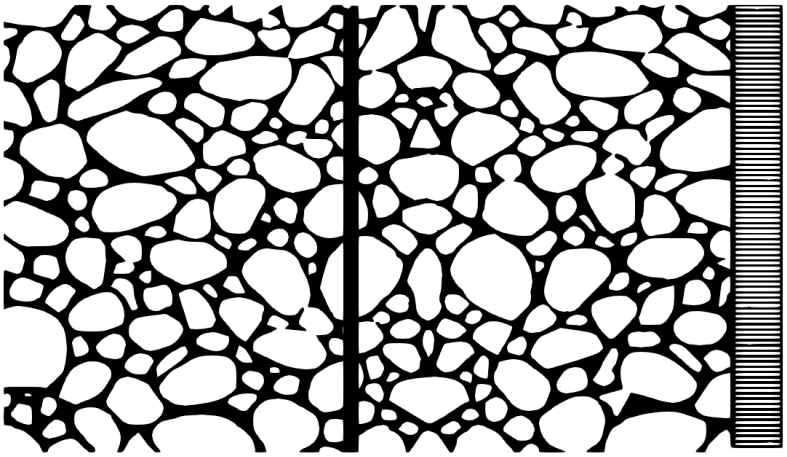

Figure 5.16 *Vertical discontinuity in the porous media in order to observe differences in capillary pressures, oil saturation and drainage time.*

As mentioned before, oil and water flow first through less pressurized zones. By adding a vertical discontinuity in the middle of the porous medium depending on its length, one can create a barrier or conduit, leading to a unique new flow pattern during the process. When adding a vertical discontinuity in the middle of the porous media, pressure along the discontinuity is the same. This causes different pressure gradients before and after the discontinuity resulting in new flow patterns as can be observed at t=1.701, see ***Figure 5.17,*** where flow takes different directions in each porous medium.

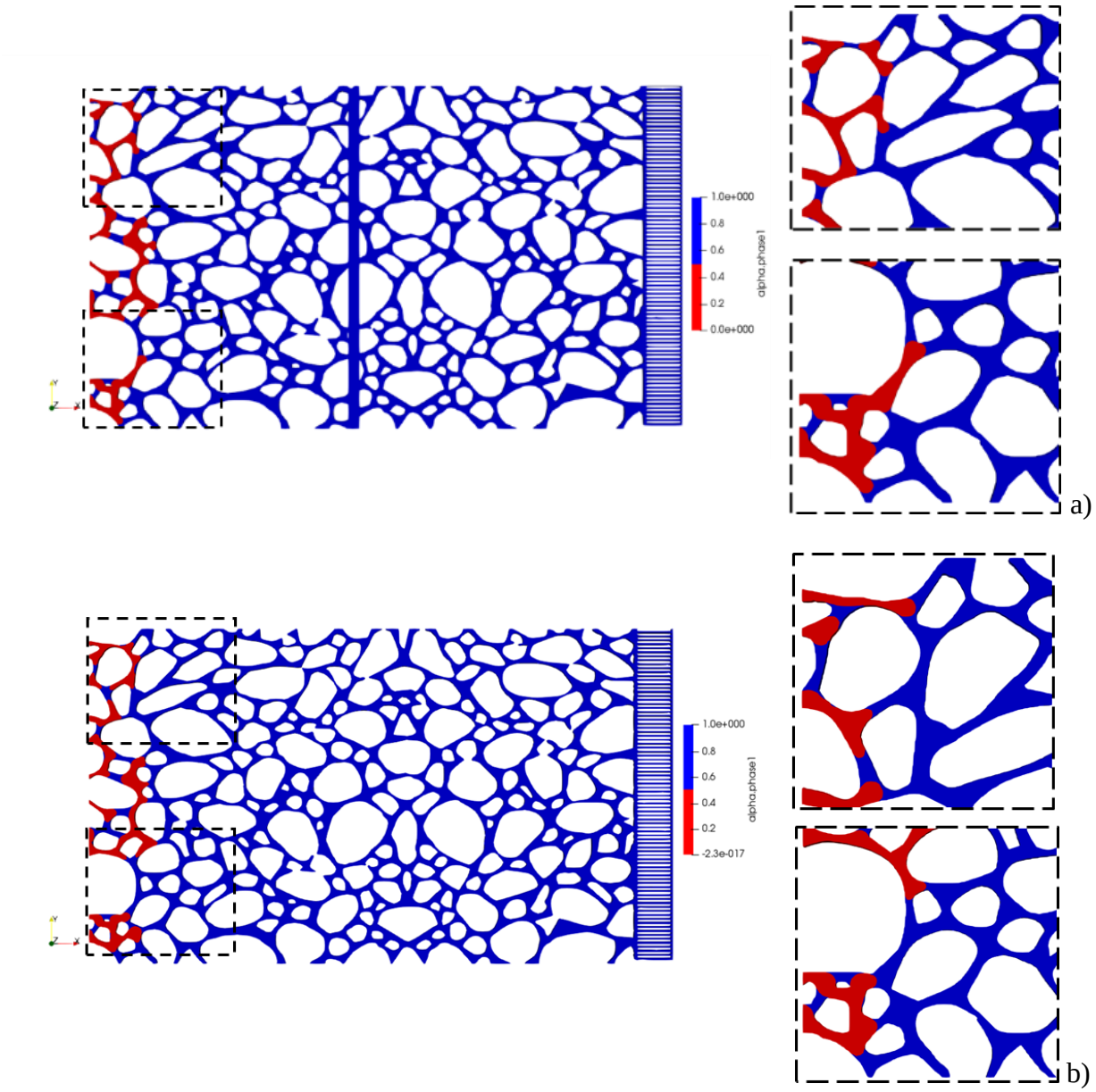

Figure 5.17 *a) Oil saturation field in vertical case (t=1.701s). b) Oil saturation field in original case (t=1.7s). Both flow patterns are different; different pressure gradients along the porous are stablished.*

Few seconds before oil reaches the vertical discontinuity, at *t*=3.9s, see ***Figure 5.18***, just one oil stream path is active while in the "no discontinuity, 1mPas" case three oil streams are active. This means that this vertical discontinuity has smaller width that some pore throats inside the media, hence, instead of being a conduit it works as an additional flow barrier.

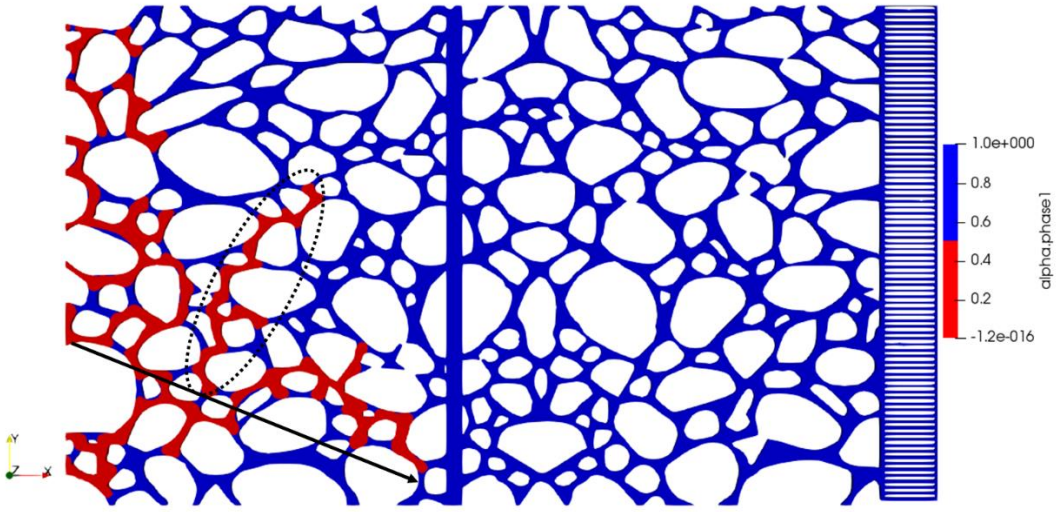

a)

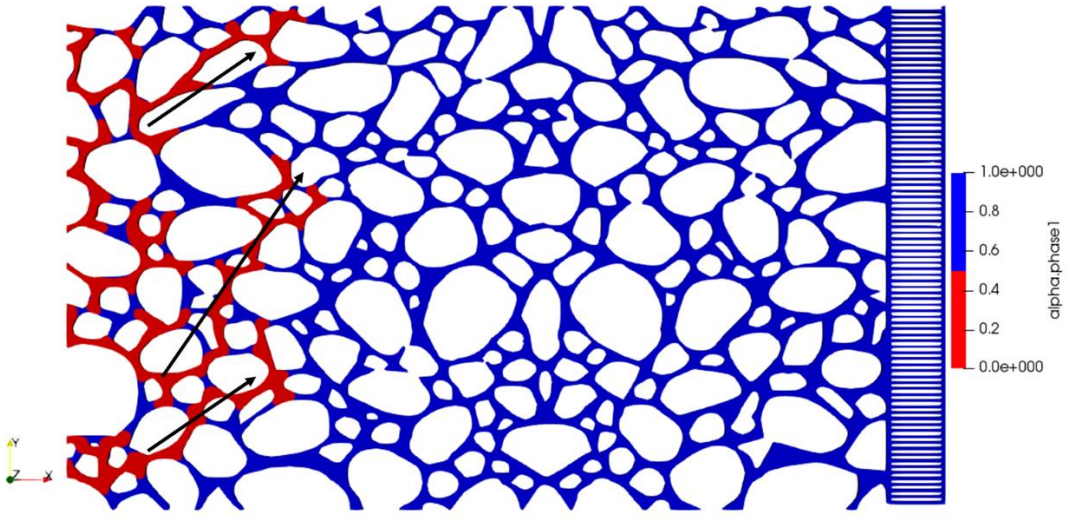

b)

Figure 5.18 *Oil two oil fingers are active flow patterns in the vertical case (t=3.901). b) Oil flow pattern in original case (t=3.908s). The vertical discontinuity works as a flow barrier, less oil fingers are active.*

Once oil reaches the vertical discontinuity, pressure decreases from 8,670Pa to 3,459Pa. After the vertical discontinuity is drained a similar pressure behavior as "no discontinuity, 1 mPas" case is observed, but the S_{wir} is lower than previous cases.

When the discontinuity is filling, a poor water displacement is noticed in the left side of the discontinuity, the narrow vertical discontinuity functions as a barrier, hence oil displacement is difficult from inlet to the discontinuity. The discontinuity is filled from bottom to top, it has to travel a long distance to arrive to top. Oil situated inside the vertical discontinuity has the same pressure along it, working as a new inlet in the system. Then a more stable displacement is noticed when draining from the vertical discontinuity to the porous plate. Oil starts draining the widest pore throats forming a preferential flow channel. At t=8.24s and P=6,381Pa, oil arrives at the porous plate, but as the porous plate function is having much smaller pores than the porous media, oil cannot cross the porous plate. Then oil flow can only continue through wider pores than the porous plate (t=9.24s, P=8,209Pa), then, when oil flows through the less resistance zones, oil drains more water, which means more sweep efficiency until at t=12.6s and P=12,498Pa, oil crosses the porous plate, see ***Figure 5.19***.

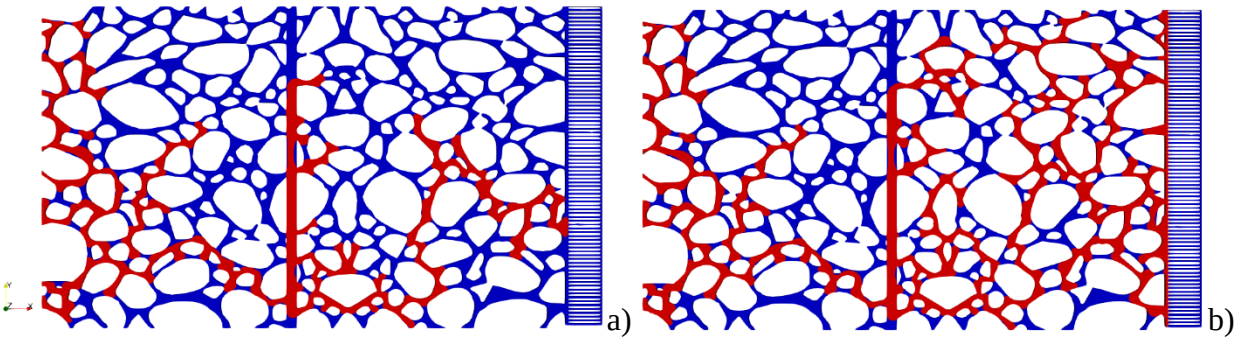

Figure 5.19 *Oil drainage process after crossing the vertical discontinuity. a)Oil starts draining the widest pore in the right side of the discontinuity, then oil moves to the next widest pore throat that allows oil passage. b)Oil arrives at the porous plate, and oil flow can only continue through pores wider than the porous plate pores and and finally oil crosses the porous plate.*

The next graph shows capillary pressure where, as mentioned above, we can observe that pressure is higher than the "no discontinuity, 1mPas" case until it finds the discontinuity where it starts decreasing while fluids flow along the discontinuity. When fluid flows along the discontinuity, pressure is very low, then increases again until fluids find the porous plate. S_{wir} is higher than the previous cases as we can be seen in ***Figure 5.20***.

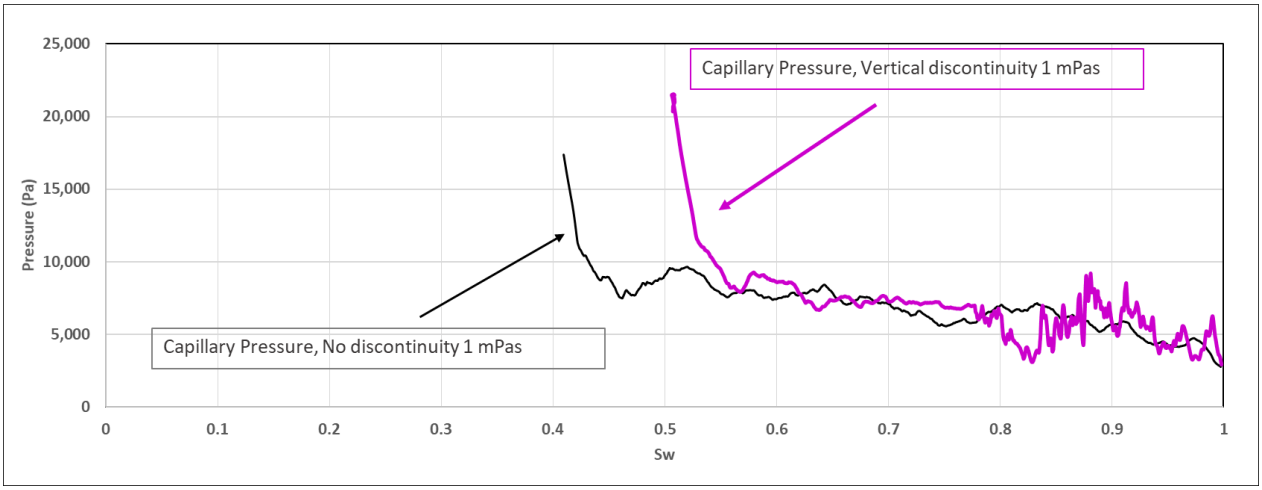

Figure 5.20 *Drainage derived capillary pressures: During oil entrance, capillary pressures are higher due to the fact that vertical discontinuity works as a vertical barrier perpendicular to flow. The lower capillary pressures are observed when oil drains water into the vertical discontinuity. Pressure along the vertical discontinuity is the same, hence a more stable displacement after draining the vertical discontinuity is observed.*

A graph of oil and water saturation versus time was done. In the first graph, we can notice that oil augments with time until no change in oil saturation is noticed. At the beginning, the oil saturation is zero S_{oi}=0 and the oil saturation reached at the end of the drainage process is S_{oi}=0.492. ***Figure 5.21*** displays the oil saturation behavior.

Comparing both cases, the case "no discontinuity, 1mPas" has more oil saturation at the end of the process, S_{oi}=0.62.

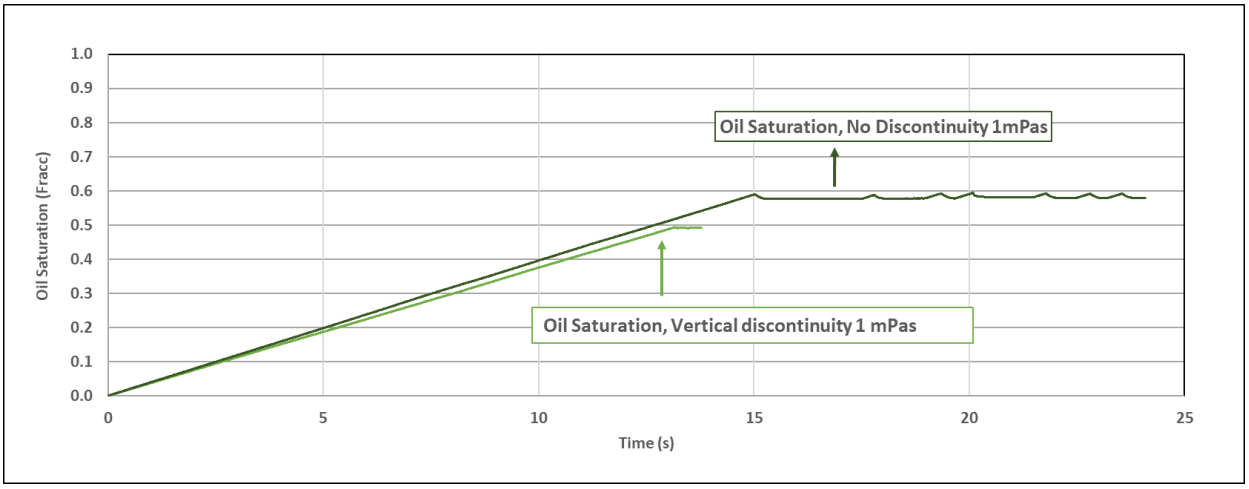

Figure 5.21 *Oil saturation behavior. Case: Vertical discontinuity, 1mPas.*

Opposite behavior can be seen in water saturation. At the beginning, water saturation is equal to 1, and the medium is fully saturated with water. As on the displacement progresses, oil saturation is reduced until the irreducible water saturation is reached. In this case S_{wi}=0.508. ***Figure 5.22*** illustrates the water saturation behaviour during drainage.

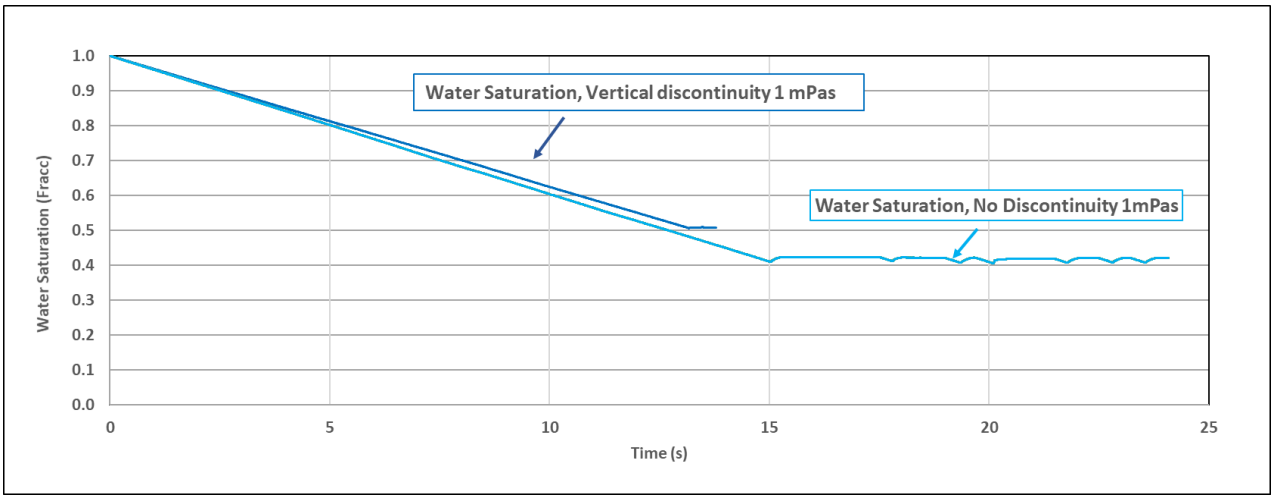

Figure 5.22 *Water saturation behavior. Case: Vertical discontinuity, 1mPas.*

5.4 Drainage in a vertical wider discontinuity, 1mPas.

A test varying the vertical discontinuity width size was done, making it 50% wider than in the last case. A 60 µm vertical discontinuity was introduced to the porous medium. In this case, a wider vertical discontinuity perpendicular to flow worked as an oil conduit, pressure along the discontinuity is lower than pressure found in the rest of the medium, hence water drainage is more efficient.

Oil enters to the discontinuity from the lower part as is noticed in ***Figure 5.23.*** At this time, we can see more water drained than in previous cases. This indicates that the width of the vertical discontinuity is larger than most of the pore throats, hence it works as a conduit. Having a discontinuity wider than some pore throats, allows oil to flow easier than previous cases leading to more drained areas.

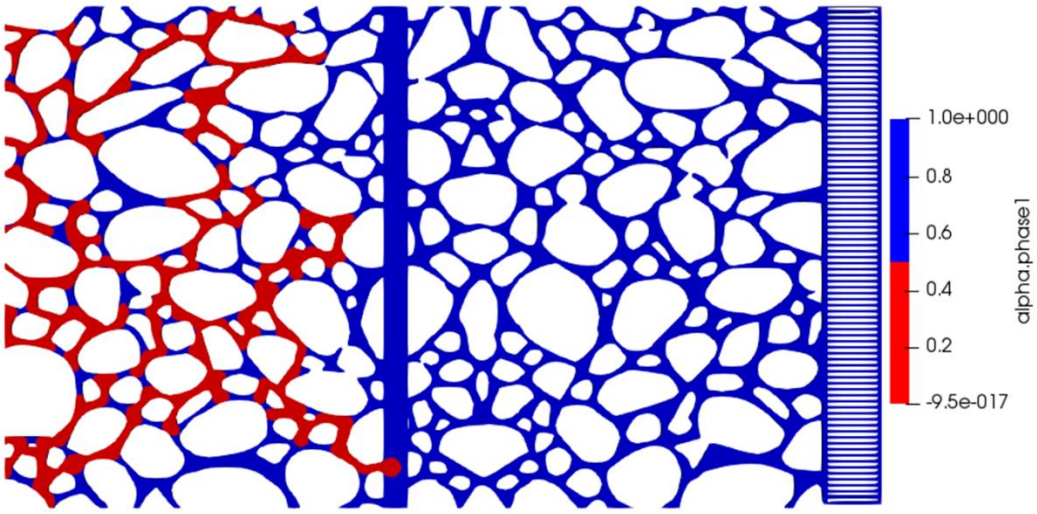

Figure 5.23 *Oil entering to the discontinuity from the lower part of the discontinuity.*

As it was mentioned, the discontinuity being wider than the pore throats, it work as a conduit, yet after the discontinuity drains, in the left side of the discontinuity the drainage continues, as we can see in, ***Figure 5.24.*** From that time on, oil advance is faster.

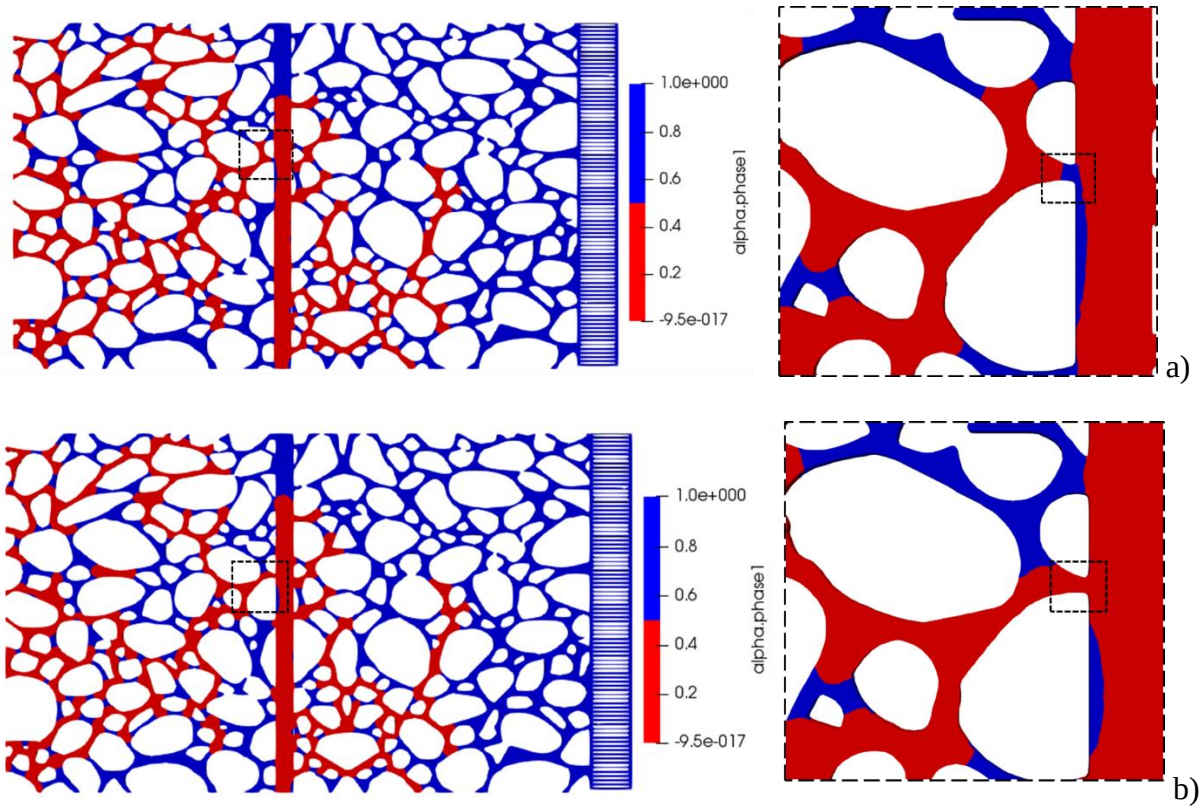

Figure 5.24 *a) b)Oil enters to the discontinuity from the middle part after oil crosses the vertical discontinuity.*

At *t*=11.03 s and *P*=7,869 Pa, oil arrives to the porous plate, as we can be observed in ***Figure 5.25*** a). At that moment, oil stops the drainage in the left part of the discontinuity and continues draining only at the right side of the discontinuity. As the porous plate function is to prevent oil flow, oil

cannot cross the porous plate, then oil flow can only continue through pores wider than the porous plate pores until oil pressure exceeds the porous plate pressure and crosses the porous plate at t=15.5s S_{wir} is reached and equal to, S_{wir}=0.42, see ***Figure 5.25*** b).

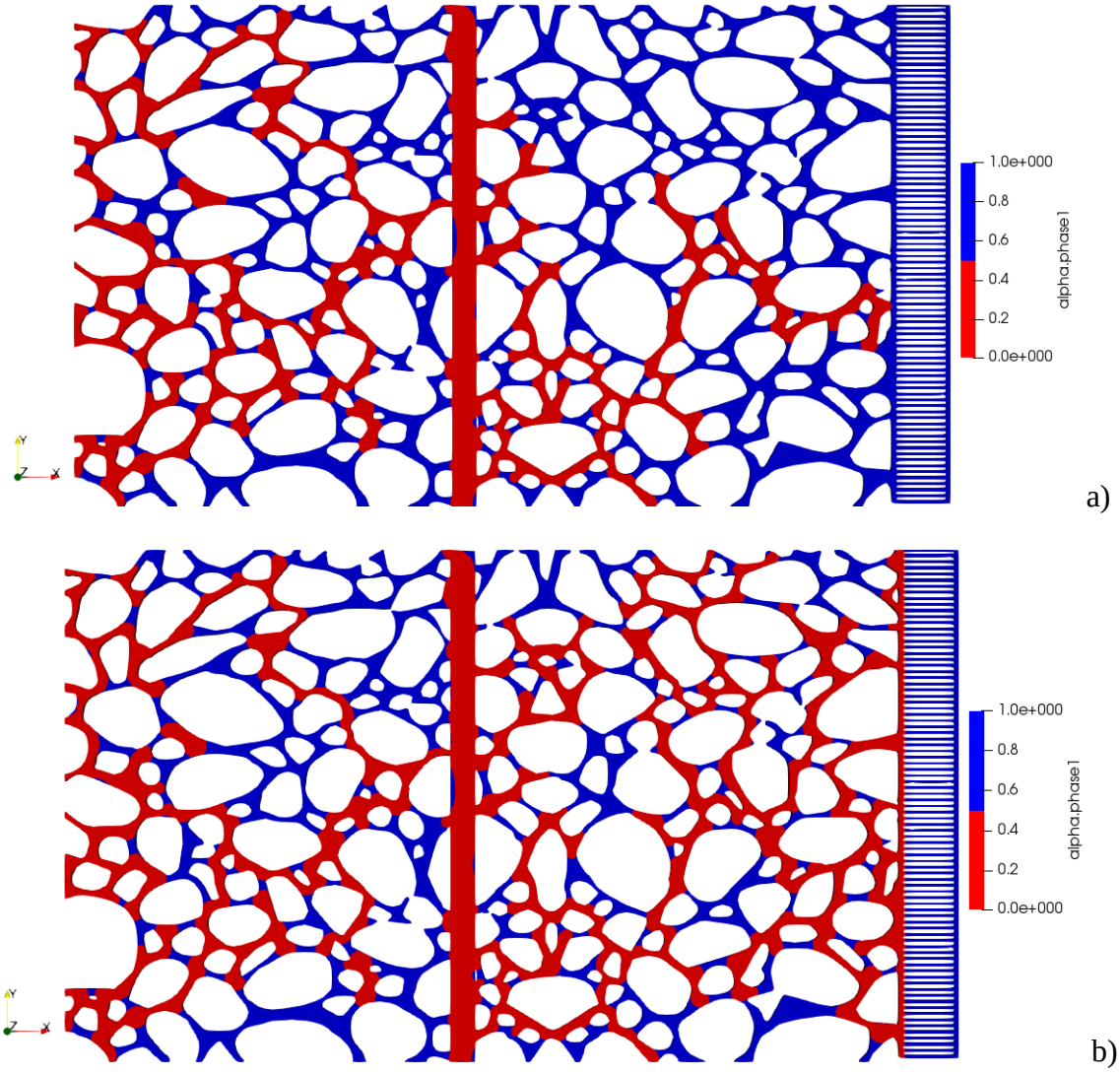

Figure 5.25 *a) Oil arriving to the porous plate. b) Oil situated along the porous plate and, S_{wir} is reached*

The next graph shows the drainage process where pressure increases until oil finds the discontinuity. When fluid flow along the discontinuity, pressure is very low, then increases again until oil finding the porous plate, a more stable displacement can be observed compared with the case "vertical discontinuity, 1mPas", it can be observed to that oil saturation is considerably lower for the actual case (S_{wir}=0.42) see ***Figure 5.26***.

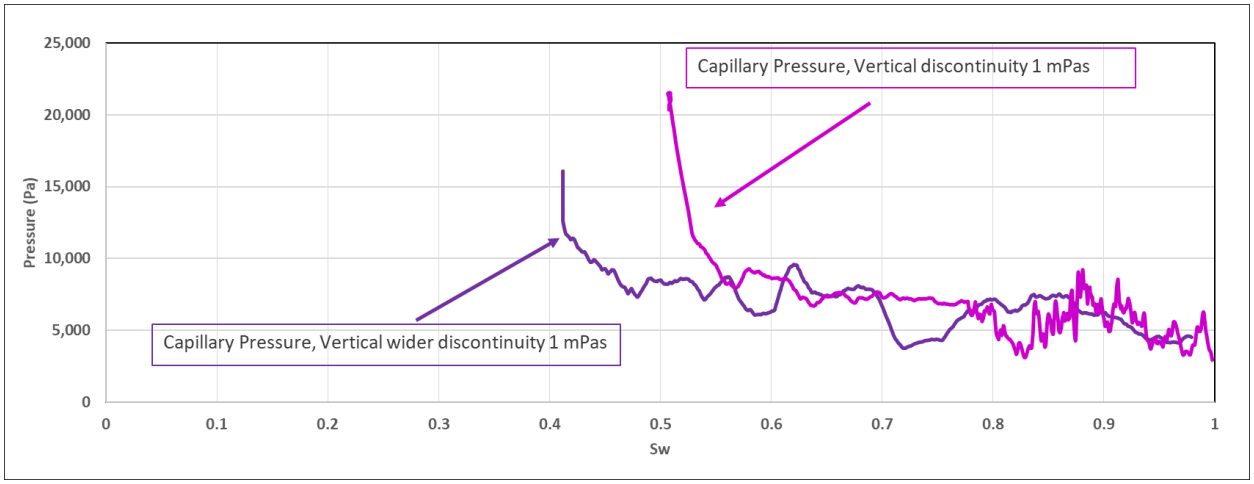

Figure 5.26 *Pressure behaviour during drainage.*

Comparing oil saturation in the last two cases with a vertical discontinuity, it can be confirmed what was mentioned in last graph. Oil saturation is slightly higher in the case "wider vertical discontinuity, 1mPas" case than the case "vertical discontinuity, 1mPas" where S_{oi}=0.51 and S_{oi}=0.58 respectively. ***Figure 5.27*** displays oil saturation response.

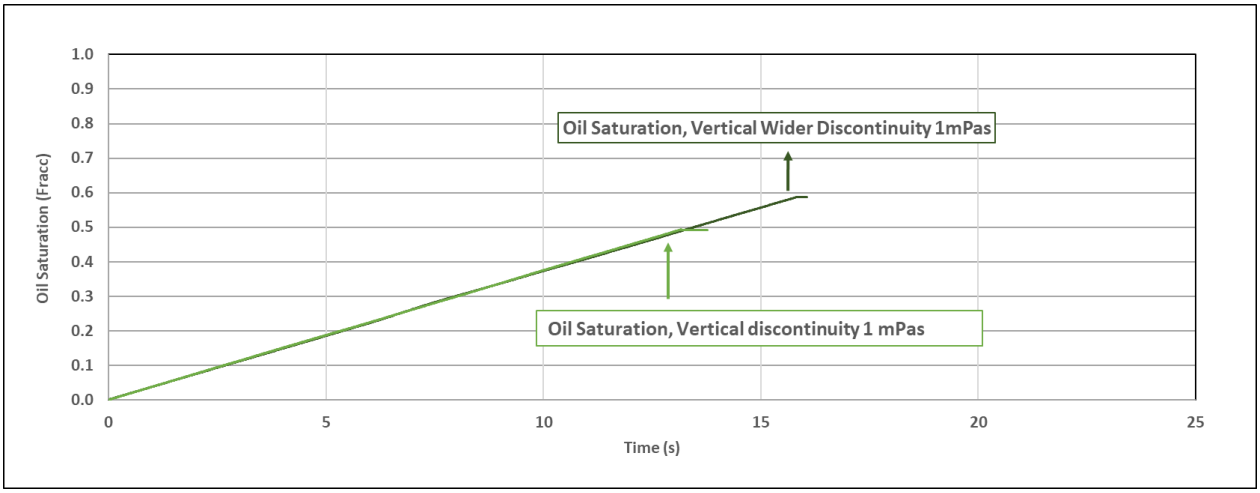

Figure 5.27 *Oil saturation vs time. Cases: "wider vertical discontinuity, 1mPas" and "vertical discontinuity, 1mPas"*

The opposite behavior can be seen in the water saturation response, as expected. At time zero, water saturation is equal to 1, the medium being fully saturated with water. As drainage time progresses, water saturation is reduced until the irreducible water saturation is reached. In the case "wider vertical discontinuity, 1mPas" the S_{wir}=0.49 and in the case "vertical discontinuity, 1mPas" S_{wir}=0.42, ***Figure 5.28*** illustrates the water saturation behaviour during drainage.

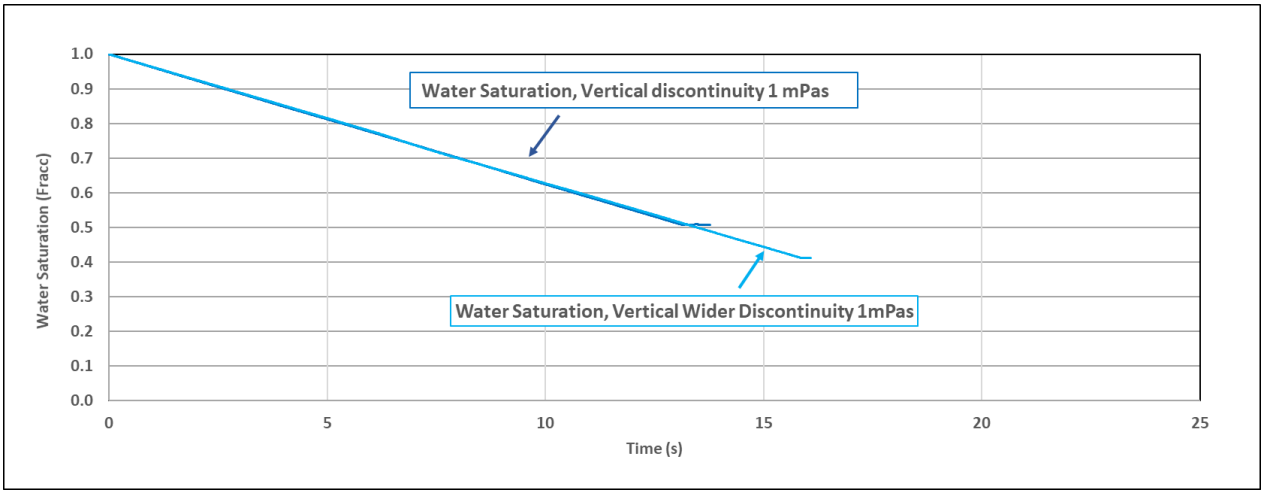

Figure 5.28 *Water saturation vs time. Cases: "wider vertical discontinuity, 1mPas" and "vertical discontinuity, 1mPas"*

5.5 Drainage in a wider vertical discontinuity. 10mPas

A test where the oil viscosity increased from 1mPas to 10mPas was run. Adding a vertical discontinuity to the porous medium changes gradient pressures inside the porous plate during drainage and increasing viscosity in the non-wetting phase increases the overall pressure needed to displace oil into the porous media resulting in higher oil saturation due to higher capillary pressures draining smaller pores.

During drainage, five oil fingers are active before oil arrives to the vertical discontinuity, as we see in ***Figure 5.29*****.** None of the four previous cases had this many capillary fingers.

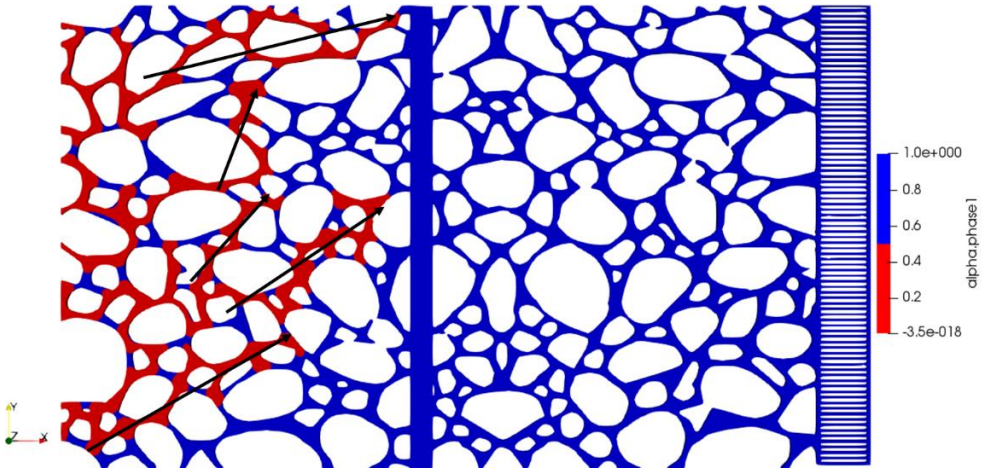

Figure 5.29 *We can visualize five oil channels heading to the vertical discontinuity.*

This pattern is similar to the previous one, where the width of the discontinuity represents a conduit. Flow heads to the upper part of the porous medium, which is a difference from the previous two cases with vertical discontinuities where the oil flow through the discontinuity was through the lower part, see ***Figure 5.30***.

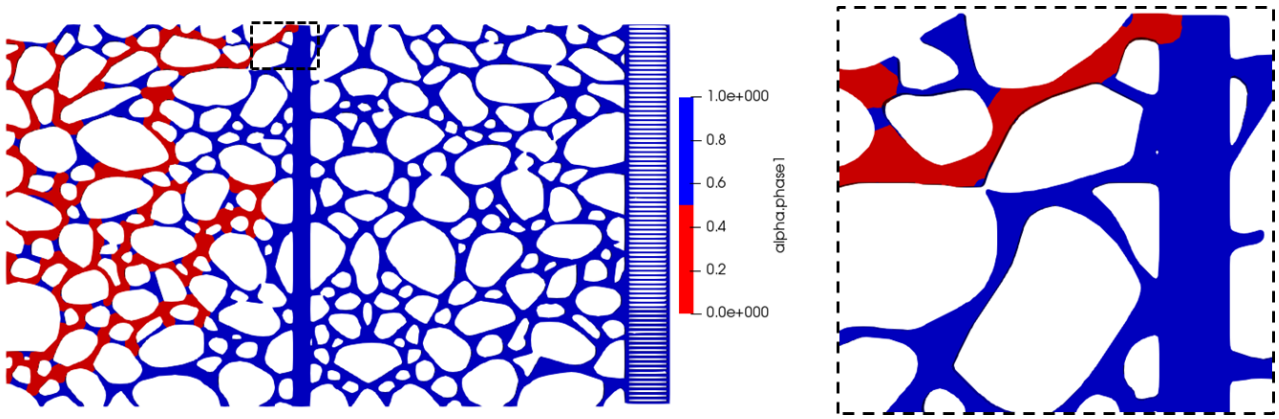

Figure 5.30 *Different from the last two cases with vertical discontinuities, oil travels through the highest part of the porous media to fill the discontinuity.*

Similar to the last case, oil keeps draining water in the left part of the vertical discontinuity even after the vertical discontinuity was drained. The vertical discontinuity width and the higher viscosity drainage causes lower S_{wir} than previous cases. We appreciate that oil mobilization throughout the porous media is more stable than the last four cases. Oil starts entering through the lower part of the discontinuity, and it starts filling faster because it has two oil entrances: the upper and lower part see ***Figure 5.31***.

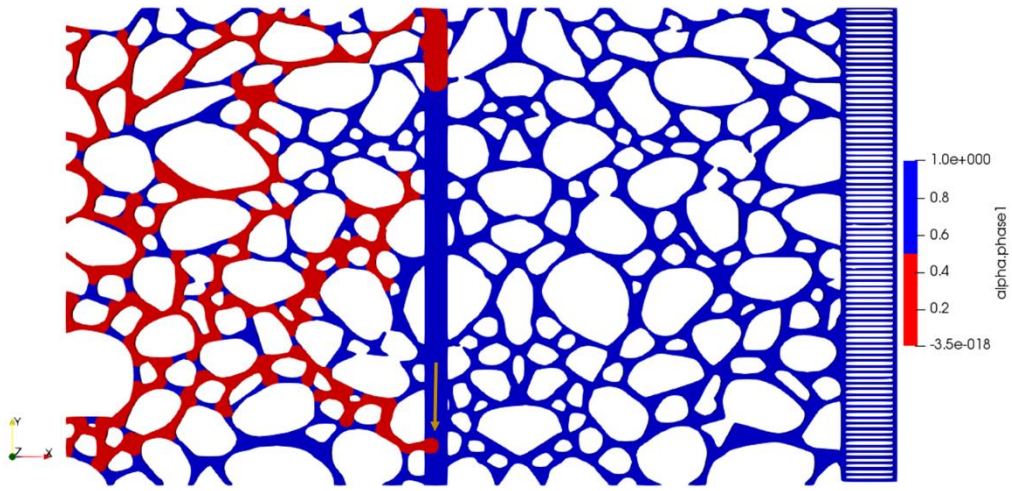

Figure 5.31 *Oil starts entering through the lowest part of the discontinuity.*

Similar to the last case, oil keeps flowing though all porous media until the porous plate is in contact with the oil,

Finally, at t=13.01s and P=10,393 Pa, oil reaches the porous plate. This is 4 seconds slower than the vertical discontinuity case and 2 seconds slower than the wider vertical discontinuous case. Oil flow continues through wider pores than the porous plate pores until oil pressure exceeds the porous plate pressure and crosses the porous plate, then S_{wir} is reached, , see ***Figure 5.32***.

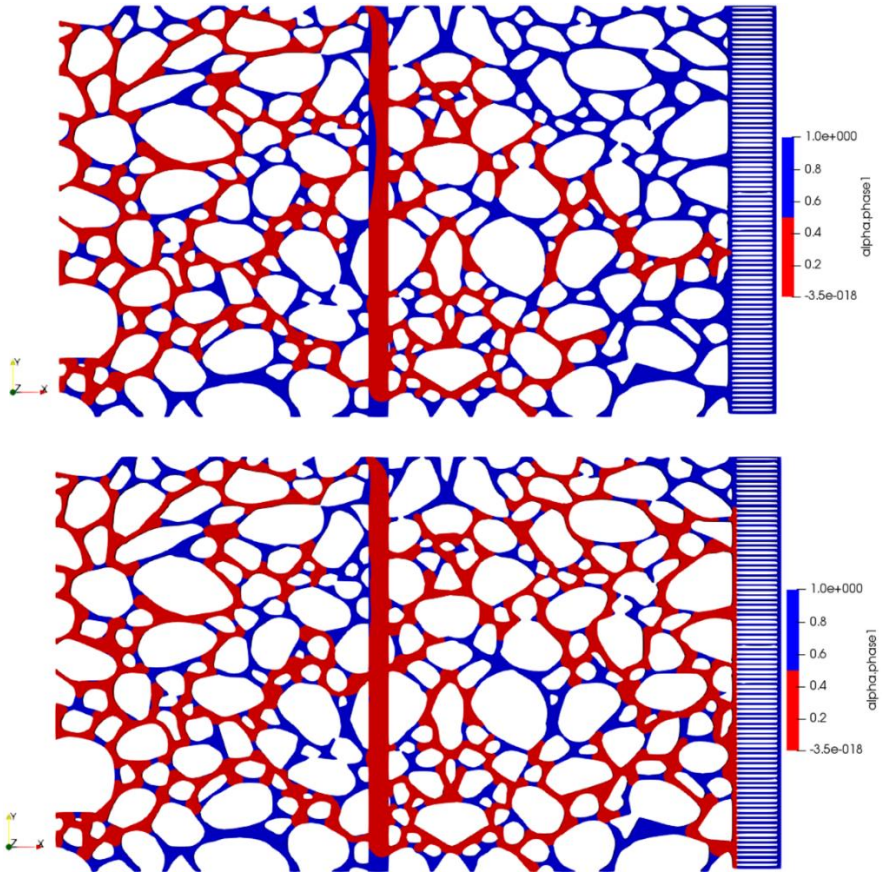

Figure 5.32 *t=13.01s. Oil film placed in front of the porous plate. b)* S_{wir} *reached, no more water flow is allowed.*

The next graph shows drainage capillary pressures where, as mentioned above, we can observe more stable pressure values. Pressure increases until oil finds the discontinuity. While oil flows inside the discontinuity, pressure decreases while oil fills the discontinuity. Afterward pressure increases again until oil reaches the porous plate, see ***¡Error! No se encuentra el origen de la referencia.***.

It can be observed that pressure behaviour in the cases "wider vertical discontinuity, 1mPas" and "vertical wider discontinuity, 10mPas" is very similar. The main difference is noticed in the water saturation during drainage in the vertical discontinuity where a higher non-wetting fluid viscosity allows higher pressures and the discontinuity is drained from the upper and lower parts achieving higher displacements. A big difference is observed in the case "vertical discontinuity, 1mPas", smaller water saturation values are seen as we can see in ***Figure 5.33***.

Speaking about arriving times, oil arrives to the porous plate at 12.6 seconds for the current case, while in the "vertical wider discontinuity, 1mPas" oil arrives to the porous plate at 15.5 seconds and in the "vertical wider discontinuity, 10mPas" oil arrives to the porous plate at 16.51 seconds.

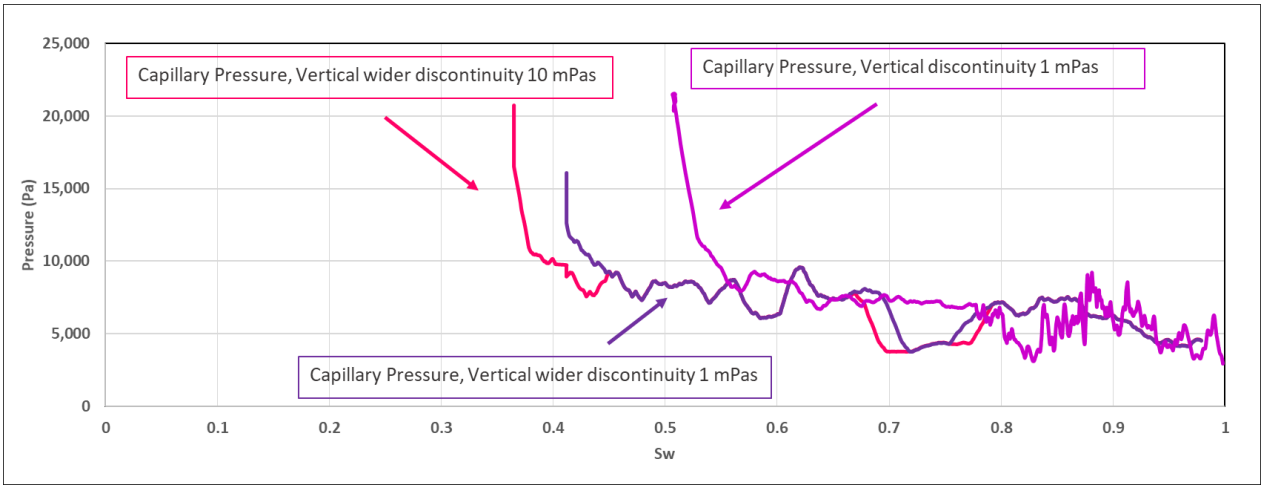

Figure 5.33 *Average pressure comparison. The pressure graph in the three cases varies in the* S_{wir}. *In the "vertical discontinuity, 1mPas"* S_{wir} *is 0.51 at P=21,396Pa, in the "vertical wider discontinuity, 1mPas" Swir is 0.41 at P=15,739 Pa and in the "vertical wider discontinuity, 10 mPa* S_{wir} *is 0.36 at P=20,365 Pa.*

In the water saturation graph, at the beginning the medium is fully saturated with water. As drainage proceeds, oil saturation increases until the irreducible water saturation is reached. In the case "vertical discontinuity, 1mPas" S_{wir}=0.49. In the case "vertical wider discontinuity, 1mPas" S_{wir}=0.59 and in the case "vertical wider discontinuity, 10mPas" S_{wir}=0.37. ***Figure 5.34*** illustrates the water saturation behaviour during drainage.

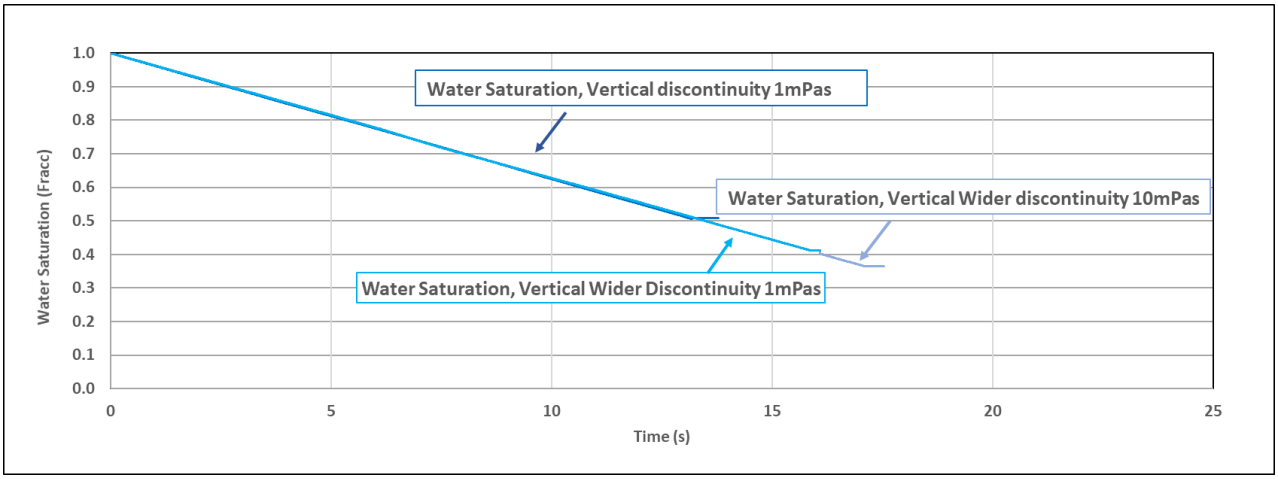

Figure 5.34 *Water saturation data for the three curves*

The opposite behavior can be seen in the oil saturation vs. time graph, where in the case "vertical discontinuity, 1mPas" S_{oi}=0.51, in the case "vertical wider discontinuity, 1mPas" S_{oi}=0.59 and in

the case "vertical wider discontinuity, 10mPas" S_{oi}=0.36. ***Figure 5.35*** illustrates the water saturation behaviour during drainage.

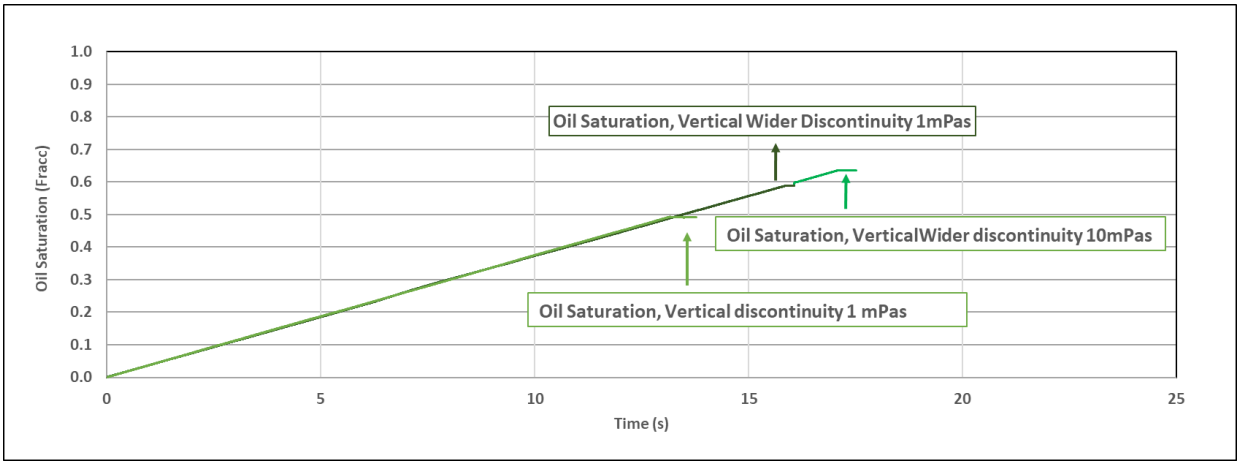

Figure 5.35 *Oil saturation vs. time graph. In the case "vertical discontinuity, 1mPas" S_{oi}=0.52, in the case "vertical wider discontinuity, 1mPas" S_{oi}=0.58 and in the case "vertical wider discontinuity, 10mPas" S_{oi}=0.63.*

5.6 Drainage in a horizontal discontinuity, 1mPas.

The addition of a horizontal discontinuity into the porous medium of 40 µm was done to investigate differences in oil breakup pressure, capillary pressure, oil saturation and porous events during primary drainage.

When adding a horizontal discontinuity from inlet to outlet, parallel to flow, fluids use it as a conduit to flow through. The horizontal discontinuity is connected to the inlet, and is wider than many of the pore throats situated inside the porous matrix. This can be observed in ***Figure 5.36.*** In the beginning more oil advances through other throats than from the discontinuity, but after some time, drainage is accomplished only through the discontinuity. When oil contacts the porous plate a flow restriction is found due to the lower permeability in the porous plate. After reaching the porous plate, oil starts draining perpendicular to its direction of flow where pore throats are wider than the porous plate, and drainage continues until no more water can be displaced.

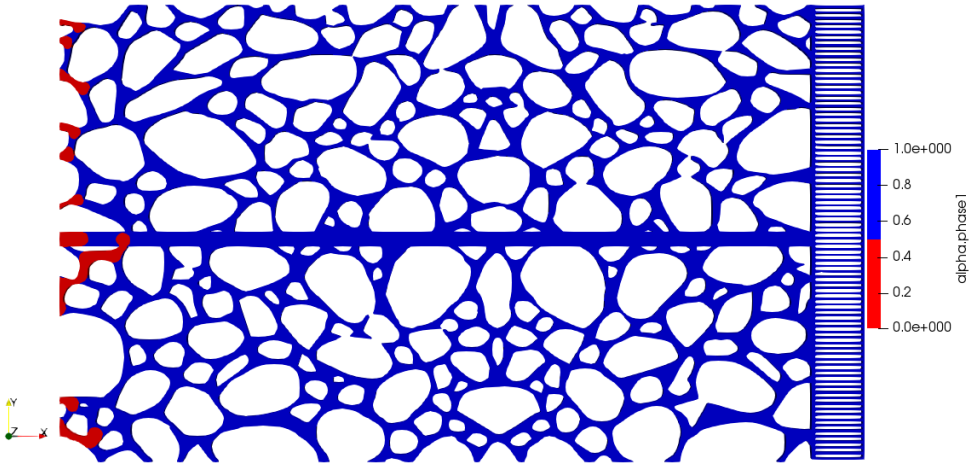

Figure 5.36 *Oil advances through a horizontal discontinuity where it functions as a conduit. Oil advance takes place from the widest pore throat to the horizontal discontinuity.*

Drainage depends on the capillary pressure of the system. Oil invades spaces where the capillary pressure is lowest, which is the largest throat connected to the inlet, until the smallest throats are filled. As we observe in ***Figure 5.37***, after some time, oil flows exclusively through the horizontal discontinuity. This means that the next element to be filled inside the porous media is smaller than the horizontal discontinuity. The lowest capillary pressure can be found along the horizontal discontinuity.

.

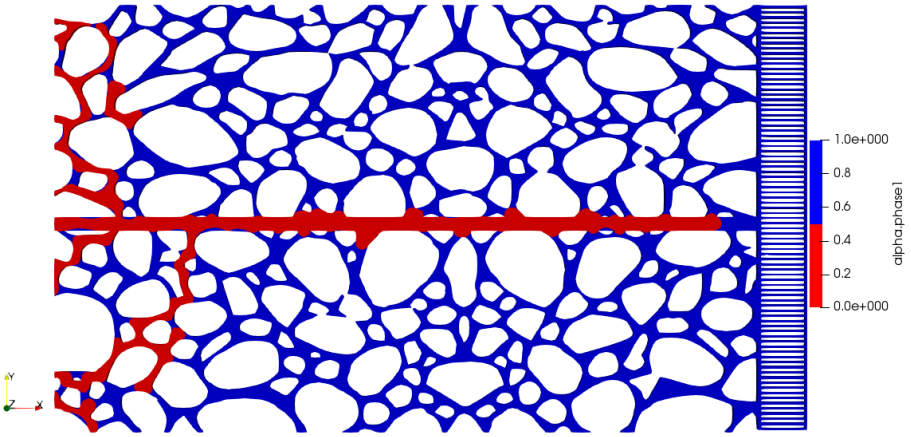

Figure 5.37. *Oil flows throughout the horizontal discontinuity.*

Finally, when oil reaches the porous plate at t=4.255, P=6,683 Pa, oil drains in all other directions where, oil finds lower capillary pressures than the ones through the porous plate, see ***Figure 5.38***.

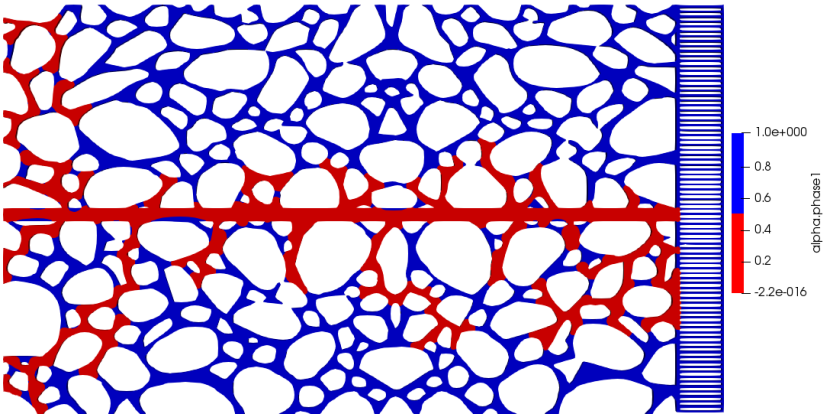

Figure 5.38 *When reaching the porous plate, oil flows, wherever capillary pressures are lower than the capillary pressure in the porous plate***.**

Finally, when no more water is displaced, S_{wir} is reached and is equal to 0.52. An oil film is created in front of the porous plate, see ***Figure 5.39***.

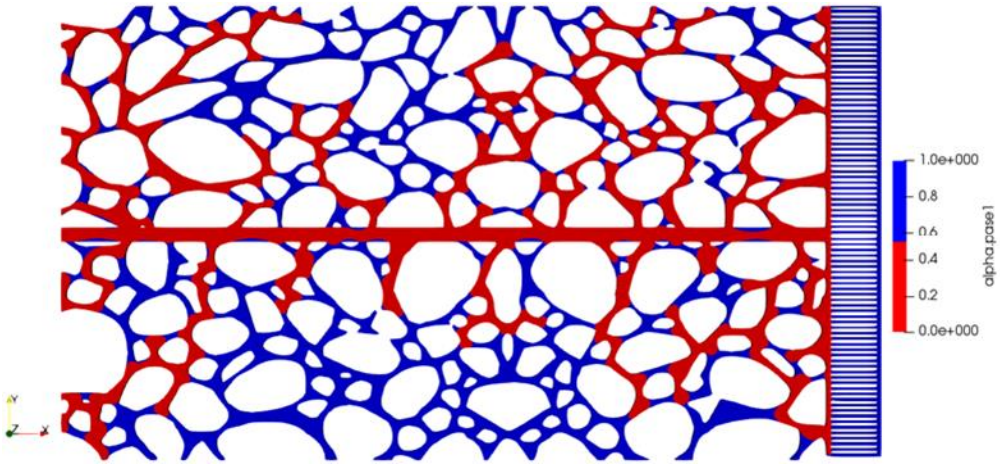

Figure 5.39 *An oil film is created along the porous plate, no more water is drained, and* S_{wir} *is reached.*

In the next graph we can observe the capillary pressure behavior. Lower capillary pressures than the previous cases are observed. S_{wir} has a value equal to 0.52 as observed in ***Figure 5.40***. The cases "no discontinuity, 1mPas", "horizontal discontinuity, 1mPas" and "vertical discontinuity, 1mPas" are plotted in the same figure to compare heterogeneity effects with the same non-wetting phase viscosity and the same fracture width. The capillary pressures obtained appear similar but not the same indicating that simple changes in geometry can significantly affect the result. This is an indication that the tested medium may not be large enough to be a Representative Elementary Volume. However it is apparently clear the heterogeneities increase the value of S_{wir} as was expected from theory.

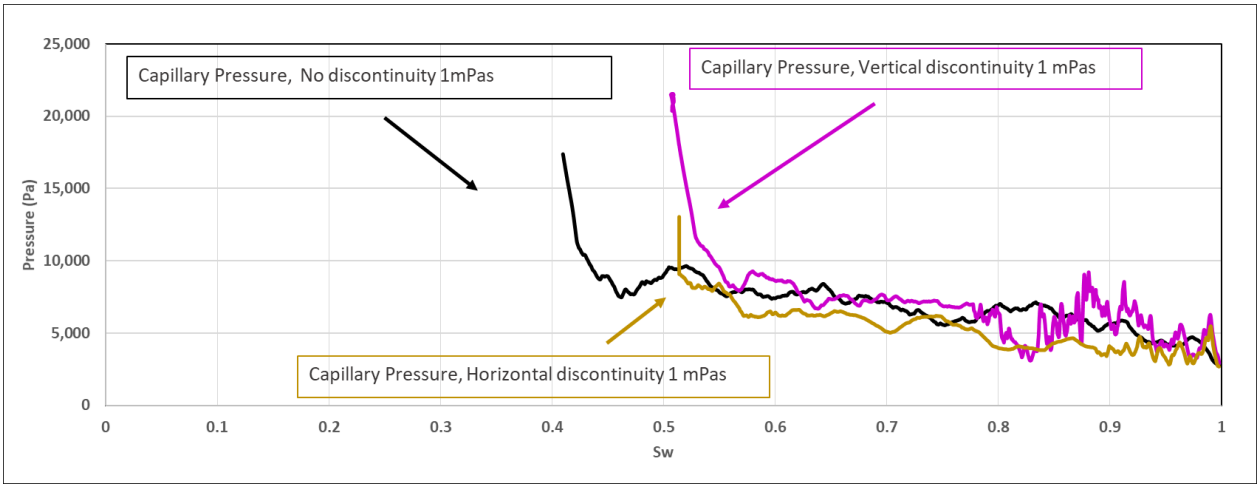

Figure 5.40 *Capillary pressures. The cases "no discontinuity, 1mPas", "horizontal discontinuity, 1mPas" and "vertical discontinuity, 1mPas" are compared..*

Looking at the oil saturation graph, we can see that oil saturation is higher in the case "no discontinuity, 1mPas", then in the case "vertical discontinuity, 1mPas", and in the last place in the case "horizontal discontinuity, 1mPas", with S_{oi}=0.58, S_{oi}=0.49 and S_{oi}=0.48 respectively, as we can appreciate in ***Figure 5.41***.

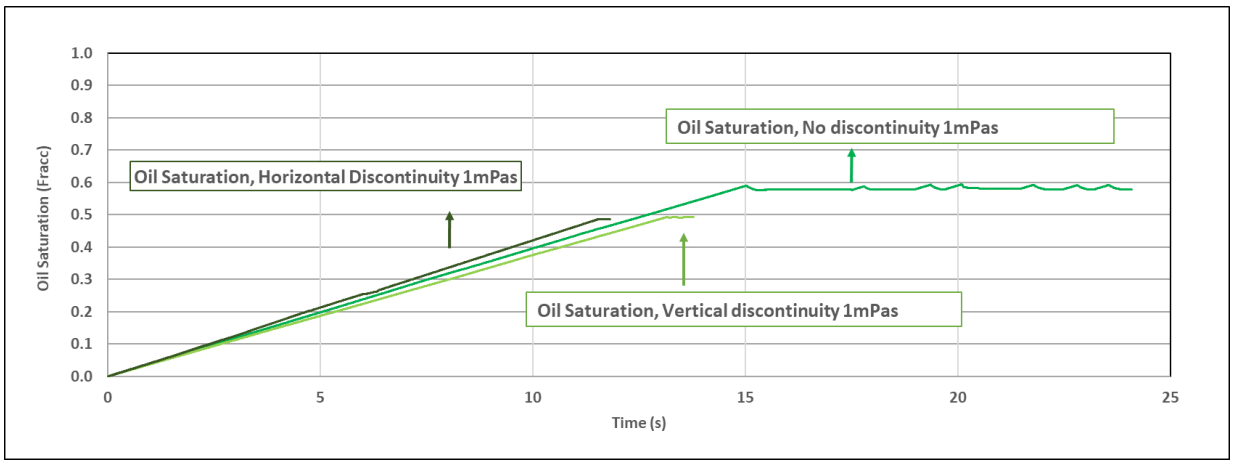

Figure 5.41 *Oil Saturation vs. time comparison. Cases: "horizontal discontinuity, 1mPas", "vertical discontinuity, 1mPas" and "no discontinuity, 1mPas".*

Looking at the water saturation graph, we can see that water saturation is higher in the case "horizontal discontinuity, 1mPas", then in the case "vertical discontinuity, 1mPas" and in the last place the case "no discontinuity, 1mPas". With S_{wir}=0.52, S_{wir}=0.51 and S_{wir}=0.42, as it can be seen in ***Figure 5.42.***

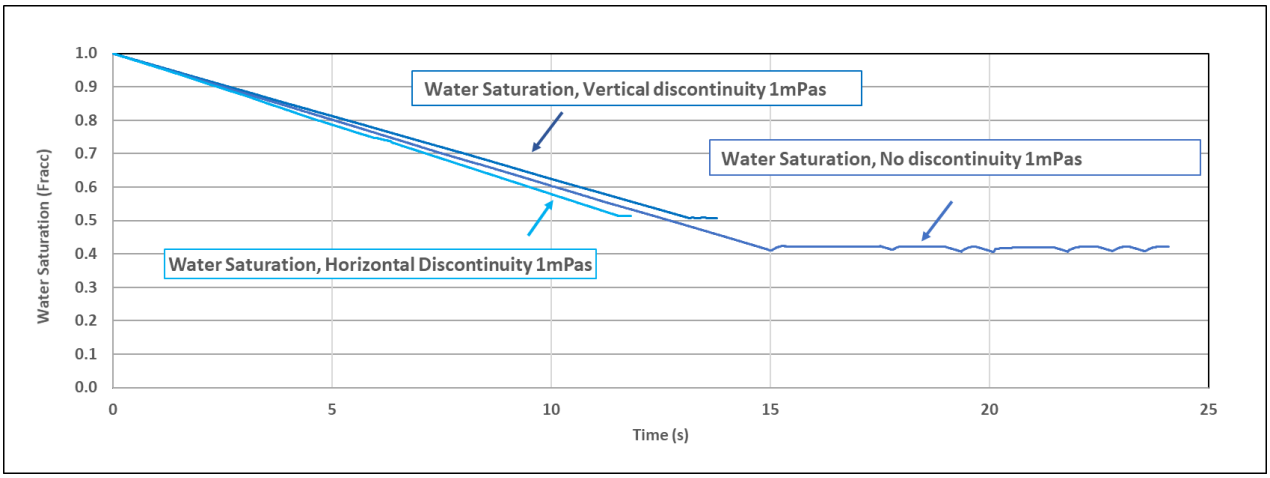

Figure 5.42 *Water saturation vs. time comparison. Cases: "horizontal discontinuity, 1mPas", "vertical discontinuity, 1mPas" and "no discontinuity, 1mPas".*

5.7 Drainage in a wider horizontal discontinuity, 1mPas.

The horizontal discontinuity width was evaluated by making it 50% wider than the last case (60 µm). Similar to the last case, since the starting point of the primary drainage fluids flow through the horizontal discontinuity where the lower capillary pressures are find, it can be observed that this discontinuity is wider than most of the pore throats inside the porous plate and just few pores are drained in the inlet. Most of the drainage is done inside the horizontal discontinuity, see ***Figure 5.43***.

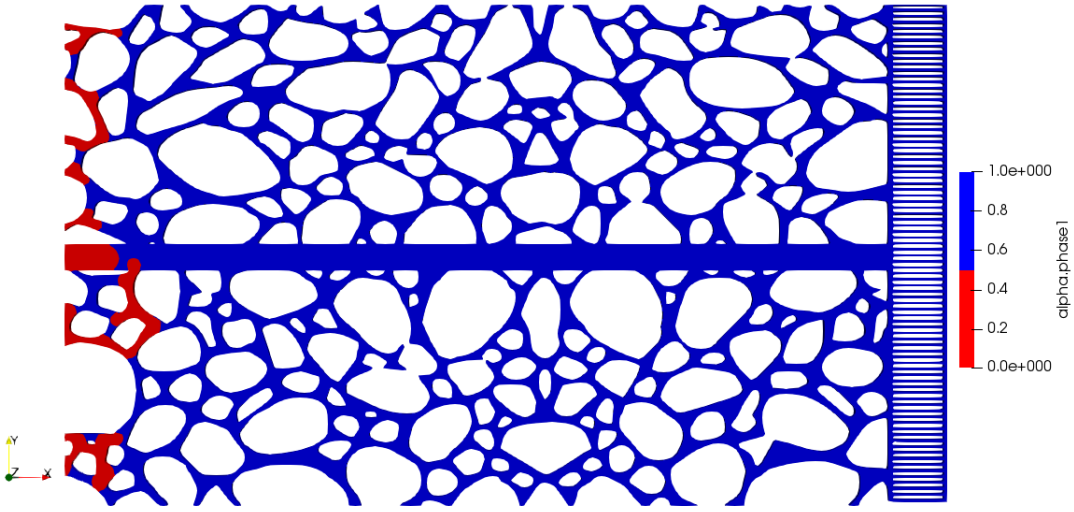

Figure 5.43 *Oil advances from the inlet to the horizontal discontinuity.*

When oil contacts the porous plate the capillary barrier is found, and water starts draining in zones with less capillary resistance until reaching the irreducible water saturation, at t=12.91s, P=8,389 Pa, S_{wir} =0.46, see ***Figure 5.44*** *and* ***Figure 5.45***.

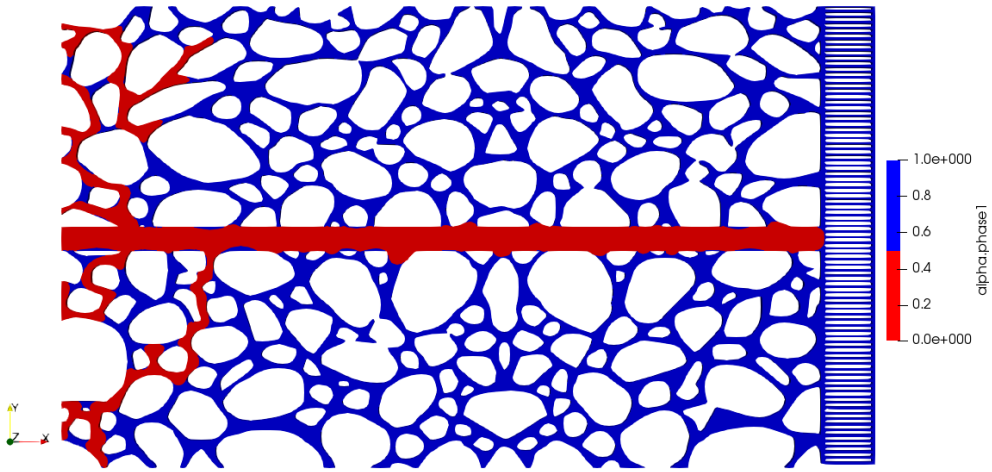

Figure 5.44 *Oil contacts the porous plate, a capillary barrier is found.*

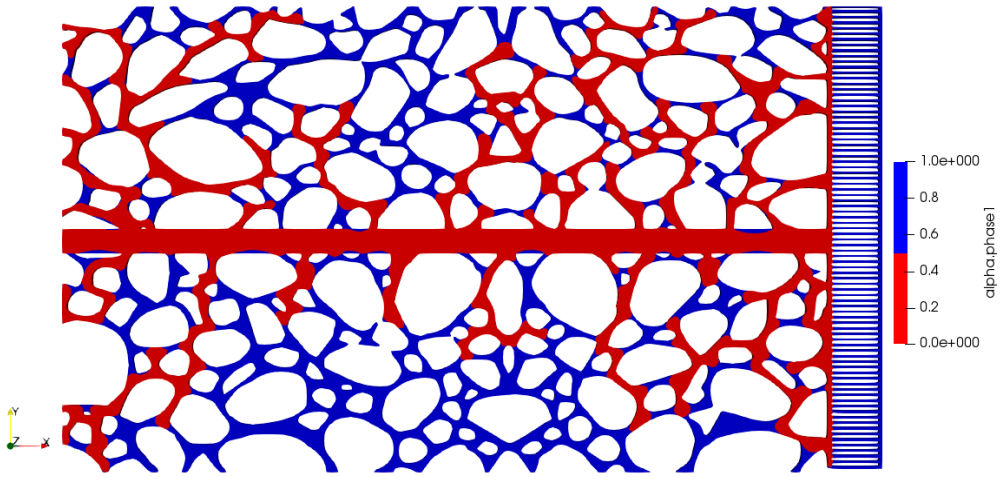

Figure 5.45 *No more water is drained, Irreducible water saturation S_{wir} is reached.*

In the next graph we can observe capillary pressure behavior in the first 1.6 seconds of the cases “horizontal discontinuity, 1mPas” “and the current case, “horizontal wider discontinuity, 1mPas” were pressure is very similar in both cases.

In the next graph we can see the full drainage process mentioned in the past paragraphs. In the first stage oil enters to the porous media. Then oil heads only through the horizontal discontinuity where the lower values of pressure are observed and in this case more water is drained because a wider discontinuity is introduced. The higher pressures are observed after the porous plate is reached and the upper and lower zones to the horizontal discontinuity are drained, until the irreducible water saturation is reached equal to 0.47.

In the graph a comparison between the cases “horizontal discontinuity, 1mPas” and the case “horizontal wider discontinuity, 1mPas” was done, where it can be noticed that average pressure is very similar in both cases. The main difference that can be seen is in the time that oil takes to drain the discontinuity. In the case “horizontal wider discontinuity, 1mPas” the width discontinuity is longer, then it takes more time to drain it than the previous case, see ***Figure 5.46***.

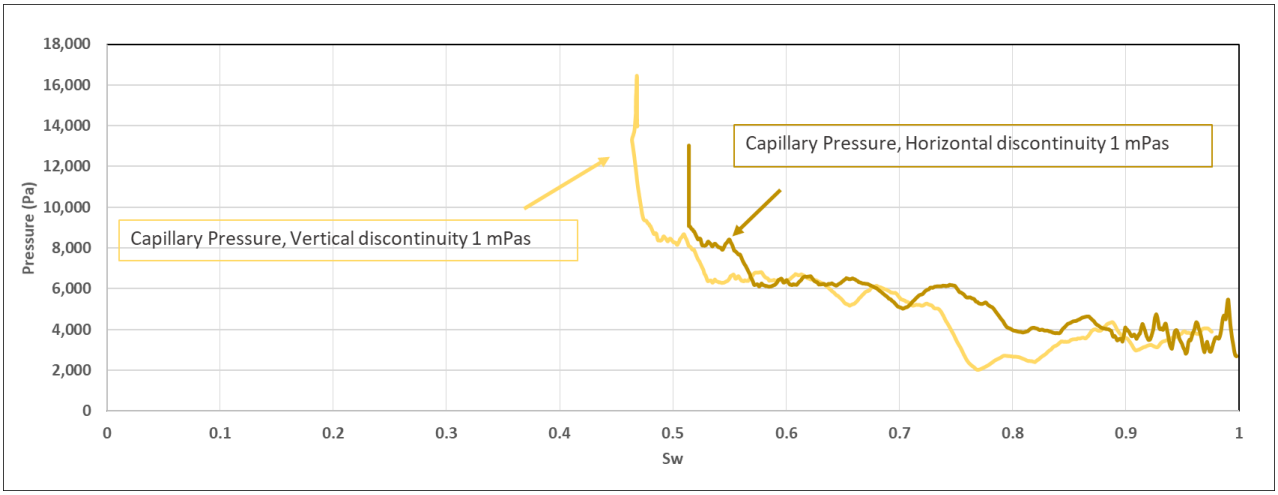

Figure 5.46 *Capillary pressure. Average pressure is very similar in both cases.*

The fact the irreducible value is lower in the case of the discontinuity is attributed to the fact the pore space in the discontinuity is sufficiently large to effect the whole pore volume.

Looking at the oil saturation graph, we can see that oil saturation is higher in the case "wider horizontal, 1mPas", than the case "horizontal discontinuity, 1mPas" with S_{oi}=0.53 and S_{oi}=0.47 respectively, as we can appreciate in ***Figure 5.47***.

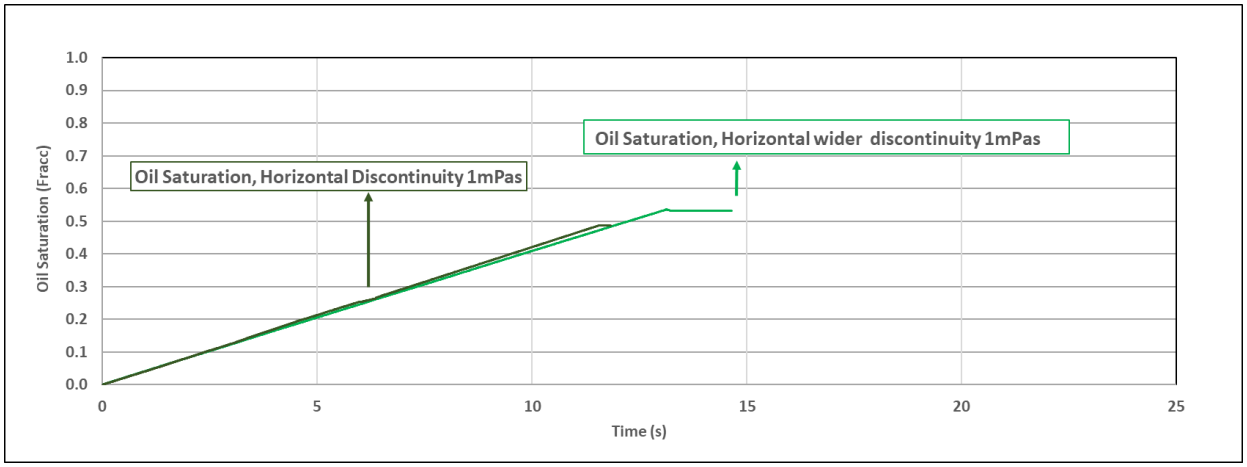

Figure 5.47 *Oil saturation vs time. Cases: "wider horizontal discontinuity, 1mPas" and "horizontal discontinuity, 1mPas"*

The opposite behavior can be seen in water saturation (as expected). In the case "wide horizontal, 1mPas" the S_{wi}=0.44 and in the case "horizontal discontinuity, 1mPas" the S_{wi}=0.52. ***Figure 5.48*** illustrates the water saturation behaviour during drainage.

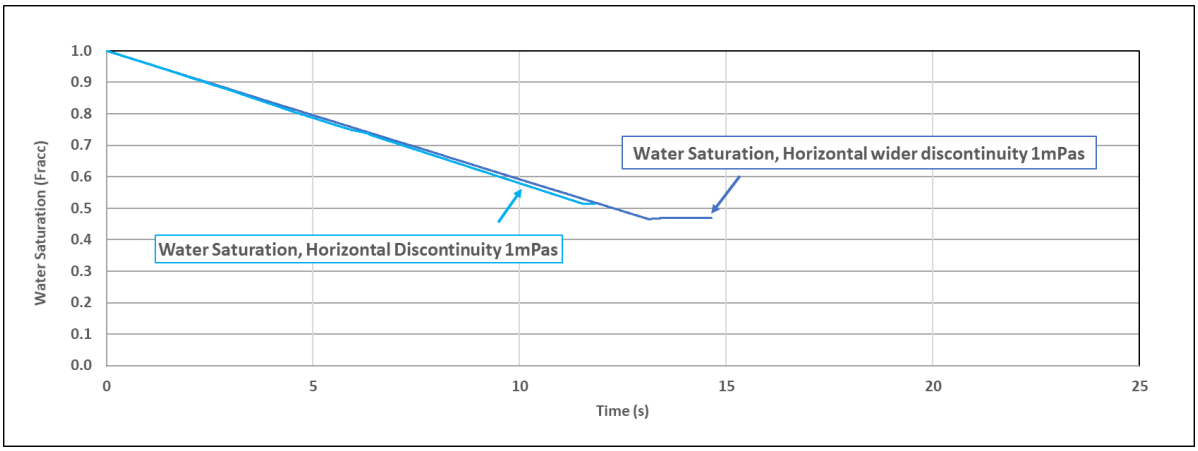

Figure 5.48 *Water saturation vs time comparison. Case: "wider horizontal discontinuity, 1mPas" and "horizontal discontinuity, 1mPas"*

5.8 Drainage in a wider horizontal discontinuity. 10 mPas

In the case, “horizontal wider discontinuity, 1mPas” a run increasing the viscosity from 1mPas to 10mPas was done. Increasing the non-wetting phase viscosity generates higher capillary pressures, hence, more water displacement is obtained.

Similar to the two previous cases, oil first drains the pores that are close to the inlet, but most of the drainage is done inside the horizontal discontinuity where lower capillary pressure values are found. After the porous plate is contacted by oil, more pores in the upper and lower part of the discontinuity drain see ***Figure 5.49.***

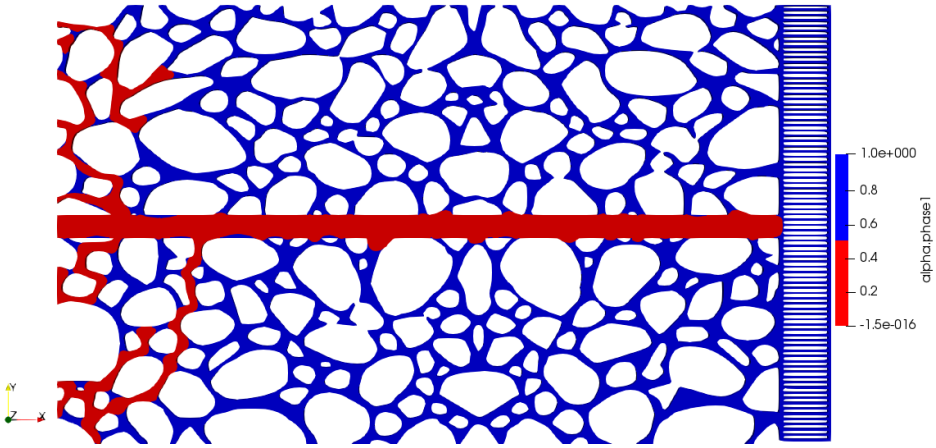

Figure 5.49 *Before oil contacts the porous plate, oil flows through the horizontal discontinuity.*

As soon as oil reaches the porous plate, oil starts the rest of the matrix, where oil finds less pressure in the system and starts draining water in zones with less capillary resistance than the porous plate until the irreducible water saturation is reached, at t=12.96s and P=9,180 Pa, where S_{wir} =0.45 as we observe in ***Figure 5.50.***

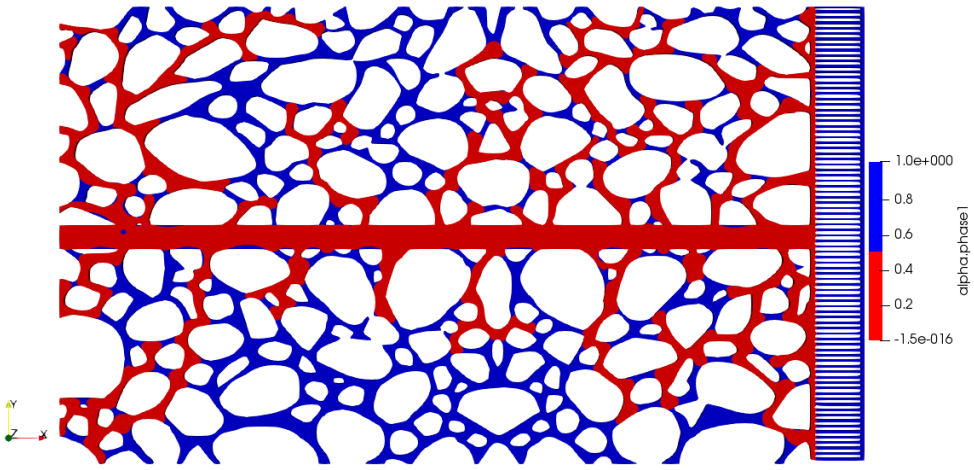

Figure 5.50 *Irreducible water saturation at t=12.96 s and P=9, 180 Pa.*

.

In the next graph we can see the full drainage process presented in the previous paragraphs. Where in the first stage the oil enters to the porous media, in the second stage oil is heading from upper and lower zones to the horizontal discontinuity, in the third stage oil is flowing through the horizontal discontinuity, in the fourth stage oil drains from the horizontal discontinuity into the matrix after contacting the porous plate, and in the fifth stage oil breaks through the porous plate

In the next graph a comparison between the cases “horizontal discontinuity, 1mPas” “wider horizontal discontinuity, 1mPas” and “wider horizontal wider discontinuity, 10mPas” is presented, where it can be noticed that average pressure is very similar in the two last cases where the horizontal discontinuities are wider. Between these cases, the main difference can be seen in the las part of the drainage, where a slightly higher capillary pressure is reached, leading in higher water drainage. For the case “horizontal discontinuity, 1mPas” drainage pressure is less stable at the early drainage stage. This case has a narrower discontinuity, meaning a lower area to flow.

Hence higher pressure when oil displaces water through it is observed and less water to drain as it can be seen in ***Figure 5.51***.

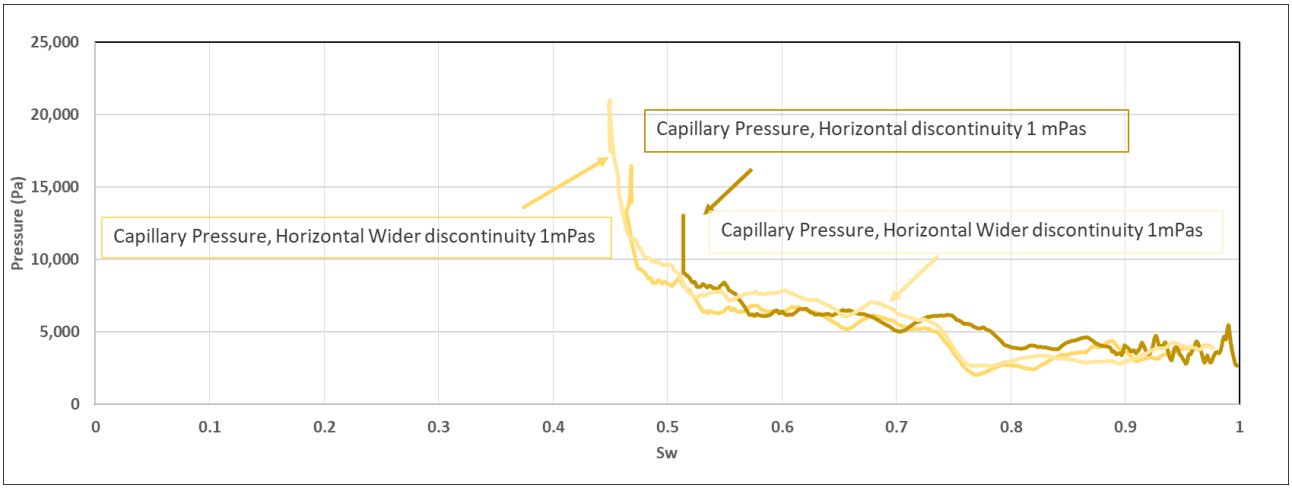

Figure 5.51 *Capillary pressure. Cases: "Horizontal discontinuity, 1mPas" "Wider horizontal discontinuity, 1mPas" and "Wider horizontal discontinuity, 10mPas". Capillary pressure is very similar in the two last cases where the horizontal discontinuities are wider. For the case "horizontal discontinuity, 1mPas" drainage pressure is less stable during drainage beginning. This case has a narrower discontinuity, meaning a lower are to flow, hence higher pressure are observed when oil displaces water through it.*

Looking at the oil saturation graph, we can see that oil saturation is higher in the case "wider horizontal discontinuity, 10mPas", then the case "wider horizontal discontinuity, 1mPas" and in the last case "horizontal discontinuity, 1mPas" with S_{oi}=0.55, S_{oi}=0.53 and S_{oi}=0.48 respectively. In the case "wider horizontal discontinuity, 10mPas" displacement pressure is higher due to higher

viscous forces when increasing viscosity, hence pores with smaller radii can be invaded resulting in slightly higher oil saturation, as can be seen in ***Figure 5.52***.

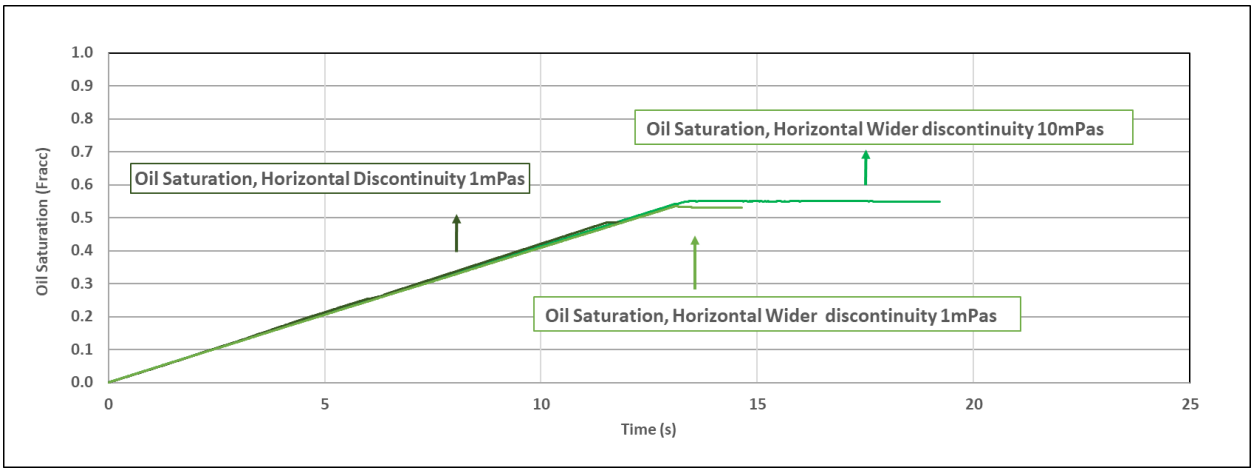

Figure 5.52 *Oil saturation vs time. Cases: "wider horizontal discontinuity, 10mPas", "wider horizontal discontinuity, 1mPas" and "horizontal discontinuity, 1mPas".*

Looking at the water saturation graph we can see that in the case "wider horizontal discontinuity, 10mPas", then the case "wider horizontal discontinuity, 1mPas" and in the last case "horizontal discontinuity, 1mPas" with S_{wir}=0.45, S_{wir}=0.47 and S_{wir}=0.52 respectively, as we can appreciate in ***Figure 5.53***.

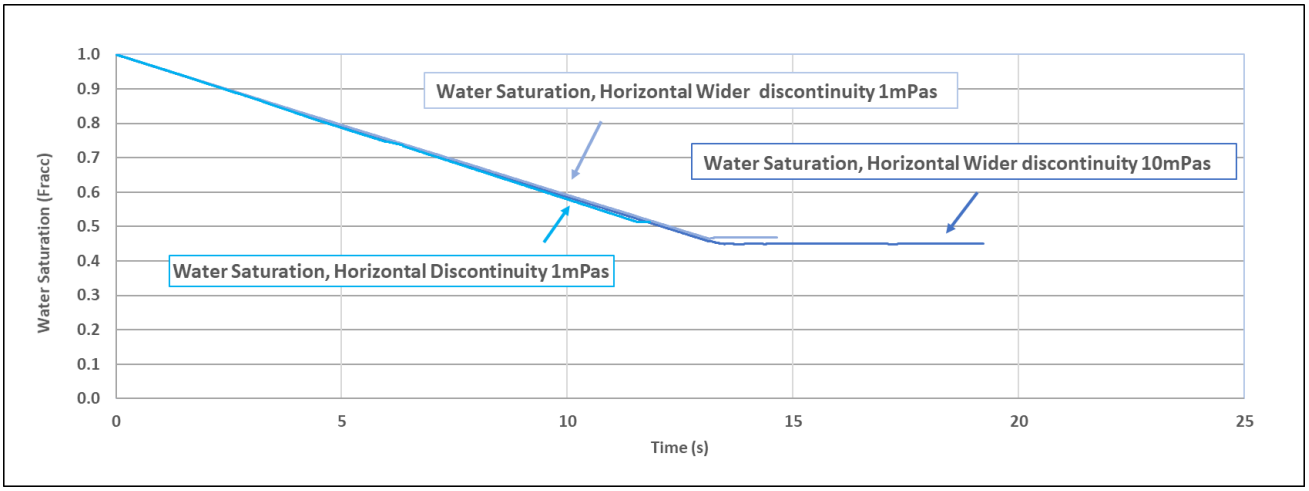

Figure 5.53 *Water saturation vs time. Cases: "wider horizontal discontinuity, 10mPas", "wider horizontal discontinuity, 1mPas" and "horizontal discontinuity, 1mPas".*

5.9 Summary

A summary of capillary pressure of the eight cases was plotted, "no discontinuity" cases are plotted in gray colors, "vertical discontinuity" cases are plotted in green colors and "horizontal discontinuity" cases are plotted in orange colors to be identified easier.

Breakup pressure is same in all cases, capillary pressures along drainage in eight cases are between 2,500 to 10,000 Pa. At the end of drainage, before capillary pressure curves tend to be vertical, a similar capillary pressure of 10,000 Pa is observed, when S_{wir} is reached.

Irreducible water saturation varies between 0.37 and 0.52. The cases with lower irreducible water saturation are the cases with no discontinuities because oil can drain since the lower capillary pressure find inside the porous media, which means bigger throat until the smaller throats are drain

until irreducible water saturation is reached meaning a good displacement process through all the porous media. Once the vertical discontinuity is drained, same pressure along the discontinuity helps to obtain a better displacement when oil heads from the discontinuity to the porous plate. The cases with higher irreducible water saturations have an horizontal discontinuity because this discontinuities starts from inlet to outlet working as a conduit, where lower drainage inside the porous media can be done, then, most of drainage is inside the horizontal discontinuity leading lower displacements through the porous media, see ***Figure 5.54***.

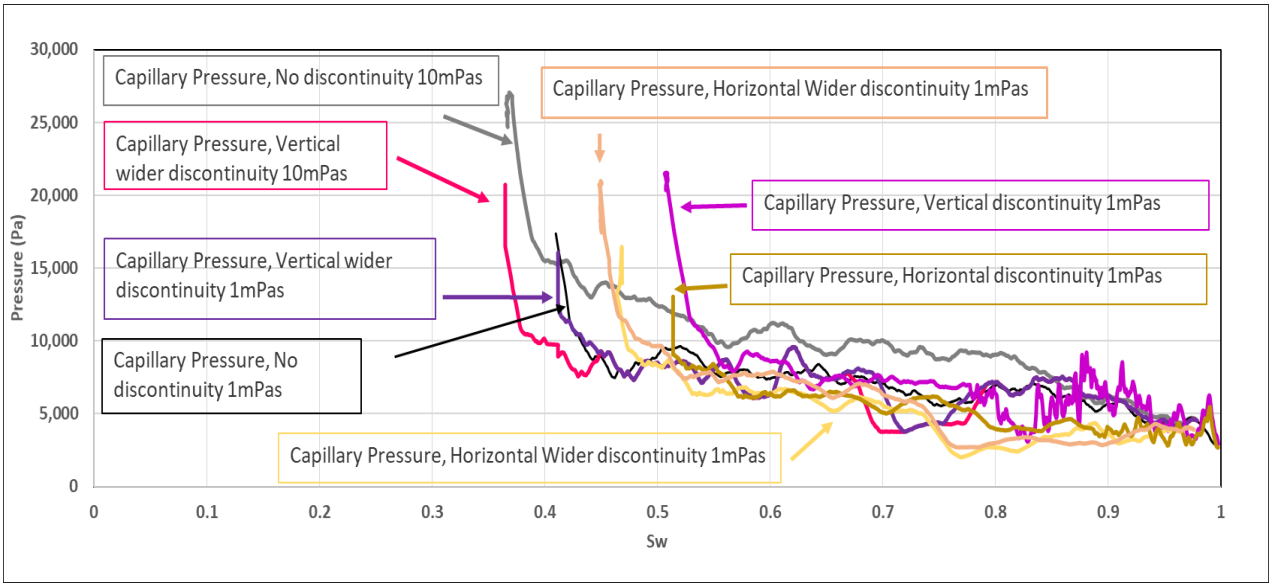

Figure 5.54 *Capillary pressure, cases "No discontinuity, 1mPas", "No discontinuity, 10mPas".*

6 CHAPTER 6: CONCLUSIONS AND RECOMMENDATIONS

6.1 Conclusions.

The simulation results demonstrate the capability to simulate primary drainage. In practical terms this corresponds to a reservoir charge, with the porous plate acting as shale cap. Many porous events could be observed such as Haines Jumps, ganglia coalescence, and drainage snap-off

The simulation was able to determine trapping in primary drainage with heterogeneities. Irreducible water saturation varies in each case depending on the pattern or the viscosity of the non-wetting phase.

The simulator was able to build a drainage capillary pressure curve, for each case.

Other conclusions seen in the simulation results:

1mPas vs 10mPas cases

For the higher oil viscosity cases, having a more viscous fluid involves higher friction between the fluid and the pore walls resulting in higher pressures to displace the oil into the porous media, higher capillary pressures invade smaller pores, resulting in higher oil saturations at the end of the drainage, simultaneously, as we see in the Lenormand´s phase diagram. The more viscous case displacements are more homogeneous resulting in more water displacement.

Drainage in a no discontinuity porous media

Comparing the cases “drainage in a homogeneous porous media, 1mPas” and the case “drainage in a homogeneous porous media, 10mPas”, most pore events can be seen in the same order, in the same zones. There are three main differences: The first one is that in the case “drainage in a homogeneous porous media, 10mPas” three main flow streams get together to form one main stream. This is different from the case “drainage in a homogeneous porous media”, where only two main streams get together and the third one disconnects from the entrance, leaving a considerable big oil ganglion trapped in the medium. This is primarily due to the lack of connectivity that can be seen in 3-D media.

The second difference is that events occur faster in the case “drainage in a homogeneous porous media, 1mPas” than the case “drainage in a homogeneous porous media, 10mPas” due to the difference in viscosities. The more viscous the nonwetting fluid, the less its facility to flow. The third one is that after breakthrough, the pressure is higher for the case of “drainage in a homogeneous porous media, 10mPas” than the case “drainage in a homogeneous porous media, 1mPas”, the more viscous the nonwetting fluid, the less its facility to flow.

Drainage in a vertical discontinuity.

In the cases “vertical discontinuity, 1mPas” and “vertical discontinuity, 1mPas”, oil enters from the lowest part of the media, while in the case “vertical wider discontinuity, 10mPas” oil enters from the top. In the case “vertical discontinuity, 1mPas” since the moment that oil touches the

discontinuity no oil drainage can be appreciated in the left side of the discontinuity, while in the cases with wider discontinuities oil drainage in the left part of the discontinuity continues until oil touches the porous plate.

Splitting this case in two parts, the first one as the left side of the discontinuity, in the case “vertical discontinuity, 1mPas” a very poor water drainage is noticed, while in the case “vertical wider discontinuity, 1mPas” the water drainage increases significantly and in the case “vertical wider discontinuity, 10mPas”, the water drainage is even more effective. And the second part, in the right side of the discontinuity, in the case “vertical wider discontinuity, 10mPas”, when oil reaches the porous plate, it spends 4 seconds more than the case “vertical discontinuity, 1mPas” and 2 seconds more than the case “vertical discontinuity, 1mPas”, as we said before. In the pressure field, we can see a considerable higher pressure in the vertical discontinuity case than the homogeneous cases.

Drainage in a horizontal discontinuity.

In the three cases of “drainage in a horizontal discontinuity” there is a big difference in pressure behavior, having the horizontal discontinuity allows fluid to flow through it since the start of the process implying lower pressure during drainage, and it increases until fluids arrive to the porous plate. When oil finally crosses the porous plate there are two behaviors: In the cases “horizontal discontinuity, 1mPas” and “horizontal wider discontinuity, 1mPas” oil flow through the porous plate is intermittent, hence pressure increases and decreases widely. This is different from the case “horizontal wider discontinuity, 10mPas” were oil flow is constant, hence pressure variation is low.

6.2 Recommendations

For future work, a 3-D model is recommended to setup, they should be different from a 2-D model.

A lower mesh refinement will give similar results accomplishing lower running time.

Higher time steps will also give similar results decreasing the running time.

Data results should be introduced in the setup in order to avoid postprocessing time and to obtain desirable results no needed to write a post processing code.

Sensibilities decreasing flow velocity can be run to observe results.

7 CHAPTER 7: REFERENCES

Al-Gharbi, Mohammed S., and Martin J. Blunt. 2005. “Dynamic Network Modeling of Two-Phase Drainage in Porous Media.” *Physical Review E - Statistical, Nonlinear, and Soft Matter Physics*.

Blazek, J. 2005. Computational Fluid Dynamics: Principles and Applications *Computational Fluid Dynamics: Principles and Applications*.

Blunt, Martin J et al. 2013. “Advances in Water Resources Pore-Scale Imaging and Modelling.” *Advances in Water Resources* 51: 197–216. http://dx.doi.org/10.1016/j.advwatres.2012.03.003.

Bruce, W.A., and H.J. Welge. 1947. “The Restored-State Method For Determination Of Oil In Place And Connate Water.” https://www.onepetro.org/conference-paper/API-47-166.

Bultreys, Tom et al. 2015. “Real-Time Visualization of Haines Jumps in Sandstone with Laboratory-Based Microcomputed Tomography.” *Water Resources Research*.

Buryakovsky, Leonid, George V. Chilingar, Herman H. Rieke, and Sanghee Shin. 2012. Petrophysics: Fundamentals of the Petrophysics of Oil and Gas Reservoirs *Petrophysics: Fundamentals of the Petrophysics of Oil and Gas Reservoirs*.

CFD Direct. 2018. *OpenFOAM Documentation*.

Chatzis, I, and F A L Dullien. 1977. “Modelling Pore Structure By 2- D and 3- D Net \ Vorks

With Application To Sandstones."

Daïan, Jean-François. 2014. "Equilibrium and Transfer in Porous Media 1: Equilibrium States Equilibrium and Transfer in Porous Media 1: Equilibrium States: Equilibrium States."

DeGance, Anthony E., and Lewis E. Johns. 1980. "On the Construction of Dispersion Approximations to the Solution of the Convective Diffusion Equation." *AIChE Journal*.

Dullien, F A L. 1992. 26 AIChE Journal *Porous Media: Fluid Transport and Pore Structure*. http://www.bvsde.paho.org/cgi-bin/wxis.exe/iah/?IsisScript=iah/iah.xis&base=bvsde.bibliografica&lang=e&nextAction=lnk&exprSearch=BVSDE.REPOLD.00055518&indexSearch=ID.

Fatt, Irving. 1956. "The Network Model of Porous Media." *Society of Petroleum Engineers Journal*.

Jakobsen, Hugo A. 2014. *Chemical Reactor Modeling. Multiphase Reactive Flows*. 2nd ed. ed. Springer International Publishing Switzerland. Springer International Publishing.

Jia, Liping, Cynthia Ross, and Anthony Kovscek. 2007. "A Pore-Network-Modeling Approach To Predict Petrophysical Properties of Diatomaceous Reservoir Rock." *SPE Reservoir Evaluation & Engineering* 10(6): 597–608.

Jim Lucas. "What Is Fluid Dynamics?" https://www.livescience.com/47446-fluid-dynamics.html.

Jordana, Carla, and Sena Santiago. 2015. "Two-Phase Flow at the Pore-Scale Using the Volume of Fluid Method."

Lenormand, R. 1990. “Liquids in Porous Media.” *Journal of Physics: Condensed Matter*.

Malvern, Lawrence E. 1969. “INTRODUCTION TO THE MECHANICS OF A CONTINUOUS MEDIUM.”

Mani, Vanita, K K Mohanty, and U Houston. 1998. “Pore-Level Network Modeling of Three-Phase Capillary Pressure and Relative Permeability Curves.” (September).

McCullough, J. J., F. W. Albaugh, and P. H. Jones. 1944. “Determination Of The Interstitial-Water Content Of Oil And Gas Sand By Laboratory Tests Of Core Samples.” *Drilling and Production Practice*: 180–88.

McPhee, Colin, Jules Reed, and Izaskun Zubizarreta. 2015. “Best Practice in Coring and Core Analysis.” In *Developments in Petroleum Science,*.

Patankar, S. V., and D. B. Spalding. 1972. “A Calculation Procedure for Heat, Mass and Momentum Transfer in Three-Dimensional Parabolic Flows.” *International Journal of Heat and Mass Transfer*.

Paul Glover. 2001. “Chapter 08 : Capillary Pressure.” *Formation Evaluation M.Sc. Course Notes*: 84–94.

Raeini, Ali Qaseminejad. 2013. “Modelling Multiphase Flow through Micro-CT Images of the Pore Space.” (March): 1–152.

Roof, J.G. 1970. “Snap-Off of Oil Droplets in Water-Wet Pores.” *Society of Petroleum Engineers Journal*.

Sahand, Etemad. 2016. “Micro-Scale Simulation of Evaporation, Condensation and Transport in Porous Media.”

Tiab, D., & Donaldson, E. 2004. *Petrophysics - Theory and Practice of Measuring Reservoir Rock and Fluid Transport Properties*.

Tsakiroglou, C D, D G Avraam, and a C Payatakes. 2004. “Simulation of the Immiscible Displacement in Porous Media Using Capillary Pressure and Relative Permeability Curves From Transient and Steady-State Experiments.” *International Symposium of the Society of Core Analysts held in Abu Dhabi*.

Tu, Jiyuan, Guan-Heng Yeoh, and Chaiqun Liu. 2009. Terror and the Postcolonial *Computational Fluid Dynamics: A Practical Approach*.